

# UC Santa Cruz

## UC Santa Cruz Electronic Theses and Dissertations

### Title

The Impacts of the 2015/2016 El Niño on California's Sandy Beaches

### Permalink

<https://escholarship.org/uc/item/2kc8c70s>

### Author

Smith, Schuyler Ann

### Publication Date

2019

### Supplemental Material

<https://escholarship.org/uc/item/2kc8c70s#supplemental>

Peer reviewed|Thesis/dissertation

UNIVERSITY OF CALIFORNIA

SANTA CRUZ

**The Impacts of the 2015/2016 El Niño on California's Sandy Beaches**

A thesis submitted in partial satisfaction  
of the requirements for the degree of

MASTER OF SCIENCE

in

EARTH SCIENCES

by

**Schuyler Smith**

December 2019

The Thesis of Schuyler Smith  
is approved:

---

Professor Chris Edwards

---

Dr. Patrick Barnard

---

Professor Gary Griggs

---

Quentin Williams  
Acting Vice Provost and Dean of Graduate Studies



## Table of Contents

List of Figures .....	iv
Abstract .....	vi
Acknowledgments .....	viii
Background/Introduction .....	1
Methodology .....	7
Results .....	12
Discussion .....	15
Conclusions .....	21
List of Supplemental Files .....	24
Bibliography .....	25
Figures .....	29

## List of Figures

Figure 1: Locations of buoys used to predict and validate nearshore wave parameters along the California coast.

Table 1: Data sources and associated uncertainty values.

Figure 1: Depiction of the spatial coverage of the different data sources used across the state of California and their associated net shoreline movement (NSM) uncertainty values.

Figure 2: Depiction of the spatial variation of uncertainty values associated with long-term rates of shoreline change.

Table 1: Mean high water (MHW) elevations for each region and associated tidal gauge measurements.

Figure 3: Map of regional boundaries determined by this study and mean high water (MHW) elevation boundaries.

Figure 5: Oceanographic forcing anomalies along the US West Coast.

Figure 6: Statewide locations of 2015/2016 El Niño net shoreline movement transects.

Figure 7: Northern California locations of 2015/2016 El Niño net shoreline movement transects.

Figure 8: Central California locations of 2015/2016 El Niño net shoreline movement transects.

Figure 9: Southern California locations of 2015/2016 El Niño net shoreline movement transects.

Table 2: Summary of statistics related to net shoreline motion values for the El Niño winter.

Table 3: Summary of statistics related to end-point rates of shoreline change from 1998-2016.

Table 4: Summary of statistics related to the satellite-derived long-term rates of shoreline change.

Table 5: Summary of National Assessment rates of shoreline change.

Figure 10: Histogram distribution of 2015/2016 El Niño winter net shoreline movement (NSM).

Figure 11: Histogram distribution of 1998-2016 end-point rates (EPR) of shoreline change.

Figure 12: Scatter plot distributions of 2015/2016 El Niño winter net shoreline movement (NSM) change values and long-term end-point rates (EPR) of shoreline change in relation to northing (UTM Y-coordinate).

Figure 13: Cumulative sum plots of **a**) net shoreline movement during the El Niño winter of 2015/016 and **b**) end-point rates of shoreline change between 1998 and 2016.

Figure 14: Scatter plot depicting the relationship between cumulative wave energy flux and net shoreline movement during the 2015/2016 El Niño winter across the state of California.

Figure 15: Scatter plot depicting the relationship between cumulative wave energy flux and net shoreline movement during the 2015/2016 El Niño winter within the Southern California Bight.

Figure 16: Map depicting 2015/2016 El Niño winter net shoreline movement values and cumulative wave energy flux values during the approximate winter shoreline change period.

## **Abstract**

### **The Impacts of the 2015/2016 El Niño on California's Sandy Beaches**

**by Schuyler Smith**

The El Niño Southern Oscillation is the most dominant mode of interannual climate variability in the Pacific. The 2015/2016 El Niño event was one of the strongest of the last 145 years, resulting in anomalously high wave energy across the U.S. West Coast, and record coastal erosion for many California beaches (Barnard et al., 2017). Currently, 26 million people live in California's coastal counties (2010 U.S. Census), and over 600,000 people in California will likely be at risk of coastal flooding by the end of this century due to projected sea level rise and storms (Barnard et al., 2019). To better manage our coastal resources, it is critical that we understand the impacts of both short-term climate variability and long-term climate impacts across the varied coastal settings of California. This study is the first to quantify the effects of one of the strongest El Niño events in the historical record across the entire coast of California, represented by 8000, 50-m spaced shore-normal transects across sandy beaches along the length of the state's shoreline.

The response of sandy shorelines to the extreme El Niño winter of 2015/2016 is quantified in the context of net shoreline movement, using the mean high water (MHW) line as a shoreline proxy. MHW contours were extracted from Light Detection and Ranging (LiDAR) digital elevation models (DEMS) from the Oregon border to Mexico using ArcGIS, to represent the 1998/2002, 2015 and 2016 shorelines. Both net shoreline movement values (from fall of 2015 to spring of 2016) and long-term end-point rates of change (1998/2002-2016) were calculated. Satellite-derived long-term (1984-2019) rates of shoreline change acquired from Luijendijk et al. (2018) are summarized for comparison. To determine the influence of wave energy on the coastal response observed here, wave energy flux values for the El Niño winter were calculated at the 20 m depth contour every 100 m along the entire California coastline using hindcast data generated by O'Reilly et al. (2016).

We find that central and northern California experienced the most sandy beach erosion during the El Niño winter, with 96% of analyzed beaches in Central California eroding (mean = 45.7 m of erosion), compared to 89% in northern California (mean = 25.5 m of erosion), and 79% in southern California (mean = 9.7 m of erosion). Although local beach response was highly variable, much of the erosion was observed at river mouths, and on the southern side of structures impeding littoral drift, with accretion observed on the northern or upcoast side of these structures. Within west-facing embayments, more extreme erosion was observed in the north than in the south. These erosional patterns contrast to those of typical El Niño events, when the direction of alongshore transport has been observed as south to north, and accretion occurs in the northern end of embayments. In the long-term (1998/2002-2016), southern California and central California beaches are moderately accreting, while northern California is eroding on average at 79 cm per year. A significant correlation was found between cumulative wave energy flux and shoreline change during the El Niño winter across the state of California ( $R_2 = -0.45$ ,  $P < 0.001$ ). The correlation is lower ( $-0.25$ ,  $P < 0.001$ ) for the 2015/2016 winter cumulative wave energy flux anomaly and shoreline change in southern California. After assessing the impact of the 2015/2016 El Niño event, spatial patterns indicate that an unusual, more northerly wave direction, extreme wave energy, and coastline orientation were key factors in the observed shoreline response. This response was markedly different from the classic El Niños of 1982-83 and 1997-98, where more southerly storm tracks and southerly wave directions were key factors controlling shoreline behavior.

## **Acknowledgments**

This work was funded by the U.S. Geological Survey (USGS) Coastal and Marine Geology Program. I wish to express my deepest gratitude to my supervisors: Patrick Barnard, Chris Edwards, and Gary Griggs, for their persistent support, open-mindedness, and confidence in my abilities. I wish to thank all of the others whose assistance was paramount in the completion of this project: Pat Limber, Paul Mattern, Henry Houskeeper, Amy Foxgrover, Li Erikson, Dan Hoover, Alex Snyder, Sean Vitousek, Andy O'Neill, Evan Dailey, and many more at the Pacific Coastal and Marine Science Center. Their technical assistance, knowledge, patience, and friendship have been invaluable. I would like to thank my cubemate, Rae Taylor Burns, for her friendship and emotional support in the final hours and for her constant willingness to lend a listening ear. I would also like to recognize Arjen Luijendijk for contributing satellite-derived rates of shoreline change, William O'Reilly for providing hindcast wave data through the California coastal wave monitoring and prediction system, Adam Young and group for providing southern California 2015 DEMs, and the USGS National Assessment of Shoreline Change team for providing constant DSAS and shoreline methodology support.

## **Background/Introduction**

Coastal California is home to some of the most popular tourist destinations in the country, as well as some of the most valuable areas of commercial and residential real estate (Heberger et al., 2011). Human populations continue to grow in these areas, with over 26 million people currently living in coastal California counties (Wilson and Fischetti, 2010). Along with residential and commercial real estate, many other types of human development exist along California's coast, including transportation systems, waste and stormwater systems, as well as oil, gas, and nuclear facilities. This level of development reflects the degree of economic activity. In fact, the activities in California's coastal counties generated \$3 trillion in GDP in 2019, a GDP that is only exceeded by four countries in the world (U.S. Bureau of Economic Analysis, 2019).

The state's coastal communities, along with their infrastructure and economies, are becoming increasingly vulnerable with climate change as accelerating sea-level rise (SLR) increases coastal flood risk (IPCC, 2007). According to California's Fourth Climate Change Assessment, it is expected that by 2050, sea level will be at least 30 centimeters higher than the sea level at the turn of the 21<sup>st</sup> century (Cayan et al., 2018). This change in sea level will threaten coastal communities across the state, with the potential to erode beaches and damage adjacent coastal property through erosion and flooding. Combined with winter storms, by 2050 it is estimated that \$32 billion in property and over 150,000 California residents would be at risk of flooding (Barnard et al., 2019). Impacts of climate change, sea-level rise, and coastal erosion also put coastal ecosystems at risk. The recent widespread loss of salt marshes and seagrass meadows are indicators of the potential for transformation, degradation, or loss of California coastal ecosystems with shoreline change (Colgan et al., 2018). Sandy beach ecosystems are particularly vulnerable to shoreline change when backed by bluffs or urban infrastructure, as there is limited room for retreat and migration of these ecosystems (Myers et al., 2019).

Shoreline change analysis is an essential tool in coastal management, engineering, and policymaking (Boak and Turner, 2005) as the shoreline serves as a suitable proxy for large-scale beach behavior (Barnard et al., 2011; Hansen and Barnard, 2010). The shoreline is formally defined as the physical intersection of land and water and is thought to have continuous spatial variation due to the dynamic nature of water levels at the coast. To analyze shoreline change, temporal fluctuations are generally measured on a time scale dependent on the context of the analysis (Boak and Turner, 2005). The USGS National Assessment of Shoreline Change Project conducts analyses of historical shoreline changes along open ocean sandy shores in California, spanning decades (Hapke et al., 2006). The most recent update determined both long-term (1800's to 2002) and short-term (1970's to 2002) shoreline change rates for the state of California, and developed standard, repeatable methods for mapping and analyzing shoreline movement. These historical, decadal change rates serve as a baseline for comparison to current shoreline change rates in California. Along with decadal shoreline fluctuations, there is a persistent seasonal shoreline oscillation in California, with accretion generally observed from June through October and erosion observed from November through May (Inman and Shepard, 1951). These fluctuations are related to seasonal shifts in wave energy, wave steepness and direction (Previsic, 2006), i.e., larger steeper waves in the winter, smaller less steep waves in the summer, with generally more extreme seasonal wave fluctuations occurring during El Niño years (Seymour, 1998).

The El Niño Southern Oscillation (ENSO) is responsible for much of the interannual climate variability in the Pacific, including sea-surface temperature and pressure variation along the equator, as well as variations in regional atmospheric and wave forcing at the higher latitudes. In particular, El Niño events produce greater deep-water wave heights and higher total water levels in the eastern North Pacific, which have been linked to increased coastal hazards during boreal winter along the entire U.S. west coast (Allan and Komar, 2006). While sea-level rise will place increasingly more stress on shorelines in the coming decades, the largest short-term shoreline changes will be observed during extreme events

such as winter storms associated with these El Niño events and very high tides, which increase the severity of coastal flooding and erosion (Barnard et al., 2015; Colgan et al., 2018).

The 2015/16 El Niño was one of the strongest El Niño events of the last 145 years (Huang et al., 2016; Wolter and Timlin, 2011), resulting in anomalously high wave energy (50% above the historical winter mean) along the coast of California and record shoreline erosion (> 70% above the historical winter mean) at 18 long-term monitoring sites scattered across the state (Barnard et al., 2017). During the 2015/16 winter, the Oceanic Niño Index (ONI), a 3-month running mean of sea surface temperature anomalies in the tropical Pacific, reached a value of 2.6, the highest in its 66-year history (NOAA National Weather Service Climate Prediction Center, 2019). The multivariate ENSO index (MEI), an indication of ENSO intensity that combines atmospheric and oceanic variables, reached a comparable value to that of the 1982/83 and 1997/98 El Niño events, which are the two other largest events since the start of MEI record reconstruction in 1871 (Barnard et al., 2017; Wolter and Timlin, 2011). Though coastal response records are limited for the 1982/83 and 1997/98 winters, these similarly powerful events are known to have caused extreme floods and weather events worldwide (Philander, 1983; Vos et al., 1999), and significant erosion across California beaches (Storlazzi and Griggs, 2000), particularly along the southern ends of littoral cells due to the more southerly wave directions (Sallenger et al., 2002). Climate change-driven changes in sea-surface temperatures and oceanic and atmospheric circulation patterns may double the occurrences of extreme El Niño events in the future (Santoso et al., 2017), potentially leading to even more severe winter storm impacts on the California coast, independent of sea-level rise. Regardless, ENSO variability has been shown to be an important driver of coastal hazards across the Pacific Ocean basin (Barnard et al., 2015), and therefore a better understanding of how California is affected during El Niño events is important for short and long-term coastal planning.

In a study by Barnard et. al (2017), a survey of six regions along the U.S. west coast (encompassing 29 beaches) revealed that during the El Niño winter of 2015/16, water level anomalies averaged 11 cm above the mean (from 1997-2016). Mean and elevated wave energy flux (a function of significant wave height and wave period; elevated representing the top 5% of wave energy flux values) were 50% above normal during the winter (December-February), resulting in winter shoreline retreat that was 76% above normal, the highest retreat ever observed. Mean and elevated wave energy flux direction during the 2015/2016 winter was close (2° and 3° more northerly, respectively) to the 20-year mean (a typically northwest wave direction) along the California coast. This is distinct from the typical southerly wave direction anomaly (averaging 6° south of the mean and as high as 13° in northern California) observed during the 1997/1998 and 2009/2010 El Niño winters across California. However, southern California experienced an even more northerly wave direction than the 20-year winter mean, with the top 5% of winter wave energy flux exhibiting an 18° and 24° wave direction anomaly compared to the El Niño winters of 1997-98 and 2009-10, respectively (Figure 1)(Barnard et al., 2017).

While the aforementioned study only analyzed 60 km of alongshore extent in California, only 5% of the total outer coast, here we document shoreline change for nearly 400 km of sandy beaches in California for the 2015/16 El Niño using airborne Light Detection and Ranging (LiDAR), representing varying shoreline orientation and levels of urbanization of the beach and backshore area. Unlike prior studies that have covered smaller, more continuous areas (Young et al., 2018a), or by proxy through a handful of small beaches (Barnard et al., 2011, 2015; 2017; Ludka, Gallien, Crosby, & Guza, 2016), this is the first study that assesses the impacts of the 2015/16 El Niño on sandy beaches along the entire state's shoreline. Given the previously mentioned value of California's coastline in terms of community, economy, infrastructure and ecosystems, it is important to assess the impacts of this particularly strong event as a proxy for shoreline vulnerability under similar and potentially more frequent El Niño conditions in the future.

## **Study Area**

Approximately 1050 km of California's coastline is comprised of low relief cliffs and bluffs, while 230 km consists of high-relief cliffs and coastal mountains. The remaining 500 km of coastline is low relief and comprised of beaches, sand dunes, bays, estuaries, and wetlands (Griggs et al., 2005). The beaches are generally short, discontinuous, and often take the form of pocket beaches, sand spits, and cusped headlands. Longer, more linear beaches, such as in Santa Monica Bay, are less frequent (Hapke et al., 2009). Due to California's size and degree of coastal geomorphic variability, the state is divided into three regions for this study: northern, central, and southern California.

Northern California has a rugged, mostly rocky coastline punctuated by a few, long stretches of sandy beaches and sand spits. Sediment is supplied mainly through streams dissecting steep coastal cliffs (Hapke et al., 2009). Central California hosts several long beaches within large embayments (e.g., Monterey Bay), as well as many pocket beaches within its stretches of high-relief coastal cliffs. River and creek outlets provide sediment to both types of beaches. The southern California coast is the most developed stretch of coastline, with coastal armoring structures widely seen and a history of coastal nourishment projects (Griggs et al., 2005). Beaches in southern California are generally long and often reinforced by jetties.

## **Wave Climate**

Northern California receives high-rainfall and wave energy, and is predominately affected by northwest swell from November to February (Storlazzi & Wingfield, 2005). Central California has a milder wave climate than the northern region and receives the most wave energy from October to April. Southern California has the most moderate wave climate of the three regions, receiving most of its wave energy from November to February. Its unique

coastline orientation and the presence of the Channel Islands acts to shelter long stretches of the shoreline from wave energy, causing alongshore variation in wave climate throughout the region (Hapke et al., 2009).

During a typical year, California receives precipitation and wave energy from the Aleutian low, a persistent zone of low pressure in the North Pacific during the winter months (Griggs et al., 2005). Waves and alongshore currents cause sediment migration in the nearshore, with a predominantly north to south direction of transport seen throughout most of the state's coastline (Hapke et al., 2009). During El Niño winters, storms have historically approached the coastline from a more southerly direction, exposing shorelines that are usually protected from a predominantly northwest swell (Sallenger et al., 2002; Storlazzi and Griggs, 2000).

Wave energy in the nearshore zone is a principal forcing mechanism for shoreline change. Thus, it is important to characterize wave climate during the 2015/2016 El Niño winter to understand the accretional and erosional patterns along the coastline during this period. While there are numerous offshore and nearshore wave buoys in California, they are limited in operational time and spatial resolution, especially in the nearshore zone after the waves have transformed across the shelf from the buoy locations. Hindcast wave data are model predictions of ocean wave conditions for past events (Barua, 2005). These provide length and continuity of wave data that may not be available otherwise. The California coastal wave monitoring and prediction system (O'Reilly et al., 2016) estimates wave conditions at the 20-m depth contour, based on deep-water directional offshore buoys (figure 2). The non-stationary, linear, spatial refraction model estimates spectral parameters, which are validated against nearshore buoy observations when available.

Through the California coastal wave monitoring and prediction system, wave conditions are estimated at 100-meter transects along the coast, a far higher spatial resolution than that of offshore wave buoys. Due to higher model skill in north San Diego County, and lower skill in southern Monterey Bay, this study highlights the correlation

between model output in southern California and its relationship to nearby shoreline change values.

In a study by Dail et al. (2000) investigating the correspondence between wave forcing and beach volume, a statistically significant correlation was found between wave energy flux and net sand volume (Dail et al., 2000) after filtering suggested by Wright et al. (1985). Additionally, a statistically significant positive correlation between wave energy flux and the Multivariate ENSO Index (*MEI*) has been identified in California (Barnard et al., 2015). Thus, wave energy flux may serve as a proxy for El Niño's impact on sandy beaches in California.

## **Methodology**

### **Data Sources**

Coastal topographic datasets used for this analysis are summarized in Table 1 and Figure 3. High-accuracy Light Detection and Ranging (LiDAR) data were downloaded from NOAA Digital Coast (NOAA Office for Coastal Management, 2019) in the form of digital elevation models (DEMs) for both pre-El Niño (2015) and post El Niño (2016), as well as 1998/2002 for perspective. Due to sparse LiDAR data coverage in southern California, southern California Coastal LiDAR from UC San Diego Library Collections (Young et al., 2018b) supplemented the pre-el Niño (2015) dataset.

Additionally, USGS data from ongoing beach morphology monitoring programs conducted at San Francisco's Ocean Beach and in Northern Monterey Bay were used to supplement the 2015 dataset (Barnard et al., 2017). Data were collected using all-terrain vehicles (ATV) with real-time kinematic global positioning system (RTK-GPS). Grids were generated from the point data, and the Mean High Water (MHW) shorelines were derived from the grids using MATLAB.

## **Shoreline Extraction and Analysis**

The Mean High Water (MHW) line is a commonly used datum-based shoreline proxy. It has definite advantages due to its lack of reliance on visual cues for interpretation (Moore et al., 2006). The MHW elevation is defined as the average of the mean high tides from local tidal gauges observed over the National Tidal Datum Epoch, currently 1983-2001 (National Oceanic and Atmospheric Administration (NOAA), 2019)(Weber, List, and Morgan 2005). Within this study, the MHW elevation in each analysis region (northern, central, and southern California) maintained consistency with that of the National Assessment of Shoreline Change (Hapke et al., 2006; Weber et al., 2005)(Table 2, Figure 4). The operational MHW line was extracted using the ArcGIS smoothed contour method (Farris et al. 2018), with the smoothing tolerance parameter set to 30 m alongshore. The smoothed contour line was then quality controlled to remove artifacts, as well as remove any contour tool interpretation of human-made infrastructure (such as jetties, piers, and sea walls), using satellite imagery from ArcGIS (Esri Inc., 2017). MHW lines were extracted from all available DEMs (Table 1).

Using the Digital Shoreline Analysis System (DSAS)(Himmelstoss et al., 2018), the 2016 MHW shoreline was buffered to create an offshore baseline. From this baseline, shore-normal transects were cast at 50-meter intervals. This baseline was smoothed with the smoothing parameter set to 300 m, after determining that this smoothing tolerance maximized transect parallelism as well as perpendicularity to the shorelines that they intersect. Due to the number of transects in this project and the coastline variability across California, there are instances in which transects are not exactly perpendicular to the shoreline. While transect orientation is generally shore-normal, it is acknowledged that net shoreline change values may reflect these imperfections in transect orientation. Current and historical satellite imagery from Google Earth (Google Earth Pro, 2016) and ArcGIS (Esri Inc., 2017) were used to manually remove transects that intersected rocky headlands, cliffs, or human-made structures without fronting beaches. Additionally, transects that intersected

primarily rocky beaches (cobble-boulder sediment size) were deleted due to lack of confidence in the ability of the MHW line to reflect shoreline change in these areas.

Within DSAS, Net Shoreline Movement (NSM) values were calculated at each transect between the pre-El Niño (2015) and post-El Niño (2016) shorelines for each region, as a proxy for sandy shoreline change throughout the El Niño winter season. The Net Shoreline Movement value is the distance between the oldest and youngest shorelines for each transect (Himmelstoss et al., 2018). For a longer-term perspective of background shoreline behavior, end-point rates (EPR) of change were also calculated between the 1998/2002 and the 2016 shorelines using the following formula:

$$EPR \left( \frac{m}{yr} \right) = \frac{NSM}{time \ between \ shorelines \ (yrs)}$$

Satellite-derived sandy shoreline change rates were downloaded for comparison to long-term end-point rates of change. Least-squares linear regression rates of change were calculated by Luijendijk from 1984 to 2016 using a fully automated method described in Luijendijk et al. (2018). Data within estuaries, large marshes, and human-made structures (such as within harbors) were removed for accurate comparison to long-term EPR of change. Positional accuracy of these satellite-derived shoreline change rates is reported in Table 5. Further details on the calculation of these uncertainty values can be found in Luijendijk et al. (2018).

### **Uncertainty**

All shoreline positional uncertainty values are reported in Table 1. The uncertainty associated with each LiDAR-derived shoreline ( $\sigma_s$ ) is comprised of the vertical and horizontal uncertainty of the DEM. It is assumed that uncertainty associated with the extraction of the MHW line from a DEM is negligible (Ruggiero et al. 2003). Using the uncertainty values

reported on the DEM metadata, the DEM vertical uncertainty was converted to horizontal uncertainty using the slope of the beach at 50-meter points along the MHW line, using the following steps: Slope maps were created from the DEMs within ArcMap using the 3D Analyst Raster Surface Slope tool. Next, the MHW lines were converted to 50-meter-spaced points, at which the slope value of the DEM was extracted. The slope value of the DEM at each point was used to convert the vertical uncertainty of the DEM to a horizontal uncertainty. These horizontal uncertainty values were averaged by region: North, Central, and Southern California. Finally, the horizontal uncertainty and converted vertical uncertainty were summed in quadrature for each region to calculate a final uncertainty value associated with each shoreline (Table 1).

For ground-based GPS (ATV) derived shorelines, uncertainty is estimated based on tests of repeatability between survey platforms and was found to be principally comprised of GPS vertical uncertainty. Factors such as the number of ATV occupants and tire penetration into sand were considered but were found to be negligible compared to the overall uncertainty of the shoreline. In Ocean Beach, the GPS vertical uncertainty is estimated to be +/- 5 cm (95% confidence interval), resulting in a cross-shore MHW positional uncertainty of +/- 28 cm (assuming a 10-degree beach face slope.)

The calculation of the total uncertainty associated with the long-term, EPR of shoreline change is outlined by The National Assessment of Shoreline Change (Hapke et al., 2006), and is calculated using the following formula:

$$EPR_{uncy} = \frac{\sqrt{\sigma_{s1}^2 + \sigma_{s2}^2}}{time}$$

Where  $\sigma_{s1}$  and  $\sigma_{s2}$  are the total uncertainty values associated with each shoreline, and  $EPR_{uncy}$  is the EPR annualized uncertainty in meters per year. Spatial variation of EPR uncertainty values is depicted in Figure 5. The total uncertainty associated with NSM values

(spatial variation depicted in Figure 3) was calculated with the same formula, but without the time value in the denominator. This is a standard error propagation formula, outlined by Taylor (1982) :

$$NSM_{uncy} = \sqrt{\sigma_{s1}^2 + \sigma_{s2}^2}$$

### **Wave Energy Correlation**

To analyze the relationship between nearshore wave energy and shoreline movement during the 2015/2016 El Niño winter, the cumulative wave energy flux was calculated using hindcast model output from the California coastal wave monitoring and prediction system (O'Reilly et al., 2016). At each 100-meter spaced transect along the coast of California, model estimates of the significant wave height ( $H_s$ ) and wave period ( $T$ ) were downloaded hourly from August 09, 2015 to April 26, 2016. This time window was chosen based on the midpoint dates of the 2015 and 2016 LiDAR data used to derive the MHW shorelines (reference to table with data sources). The cumulative wave energy flux ( $E_f$ ) was calculated at each offshore transect, using the following formula:

$$E_f = \sum \frac{\rho g^2 H_s T}{64\pi}$$

Where  $\rho=1025 \text{ kg m}^{-3}$  is the density of seawater at the surface,  $g$  is the acceleration due to gravity,  $H_s$  is the significant wave height and  $T$  is the wave period. To identify a relationship between cumulative wave energy flux and net shoreline movement (NSM) during the study period, the nearest model wave point to each net shoreline movement point was identified. The pairs of onshore and offshore points were filtered to only include pairs less than one-kilometer distance from one another.

Due to higher model skill in the San Diego area, this analysis was repeated for net shoreline points within the Southern California Bight. Cumulative wave energy flux ( $E_f$ ) data in the Southern California Bight were normalized by dividing each  $E_f$  value by the mean  $E_f$  from all winters from 2000/2001 to 2015/2016, which were calculated using hindcast data from the same date window for each year. These calculations are expressed using the following formulas:

$$\overline{X_{E_f}} = \frac{\sum E_{f_1} + E_{f_2} \dots E_{f_n}}{n}$$

$$E_{f_{norm}} = \frac{E_f}{\overline{X_{E_f}}}$$

Where  $\overline{X_{E_f}}$  represents the mean cumulative wave energy flux of all winters from 2000/2001 to 2015/2016, and  $E_{f_{norm}}$  represents the normalized cumulative wave energy flux for each offshore transect. To ensure analysis of only NSM points that were influenced by waves rather than strong tidal currents and river fluxes during the El Niño winter, satellite imagery from Google Earth (Google Earth Pro, 2016) was used to identify shoreline change points located at river mouths in the 2015. These NSM points were then removed from the southern California dataset (2.2 percent of the dataset was removed). NSM points were then filtered for proximity to corresponding  $E_{f_{norm}}$  points, eliminating any pairs greater than 1 km distance from one another to ensure accurate comparison. Outliers representing 1.5% of the filtered dataset were eliminated by filtering for pairs of points in which  $E_{f_{norm}}$  was less than 0.7.

## Results

### Net Shoreline Movement and End Point Rates

Within northern, central, and southern California, 76, 52, and 281

km of sandy beaches were analyzed for net shoreline movement (NSM) during the El Niño winter, respectively. Spatial coverage of the NSM analysis is depicted in Figures 6 through 9. Supplemental figures 1 through 4 depict more detailed NSM rates of change in various areas of interest. Throughout this section, uncertainty values of change rates are left out of the text for clarity; however, they are reported in Tables 3 through 6, along with the rest of the results. The long-term, 1998/2002 to 2016 end point rate (EPR) analysis encompassed 101, 187, and 341 km of sandy beaches in the three respective regions. Statewide, 83% of the transects were found to be erosional during the El Niño winter of 2015/2016, while only 52% of long-term (1998/2002-2016) transects were found to be erosional. Figures 10 and 11 depict histogram distributions of NSM and EPR change values.

In northern California, sandy shorelines eroded an average of 25.5 m during the El Niño winter of 2015/2016 (NSM)(Figure 10(a)). The maximum winter erosional value reached 148.6 m on the southern end of Pudding Creek beach in Fort Bragg, which was the most extreme incident of erosion statewide. The maximum shoreline accretion value was 61.9 m, which occurred on a sand spit in the center of the mouth of the Klamath River. 89% of winter (NSM) transects were erosional, and 11% of transects were accretional or stationary. In contrast, in the long-term (EPR, 1998/2002-2016) 70% of transects were eroding and 30% were accreting or stationary. This is the highest percentage of transects eroding in the long-term (1998/2002-2016) out of all three regions. However, it should be noted that northern California had the least amount of transects analyzed for this long-term (EPR) change, due to the limited coverage of the 2002 LiDAR survey (Table 1) as well as prevalence of high-relief, cliff back coastline. Spatial distribution of NSM values and EPR values for northern California can be seen in Figure 12(a).

Central California saw the most erosional El Niño NSM mean of 45.7 m, with the maximum El Niño winter erosional value in the region reaching 121.0 m at the mouth of Morro Creek, near Morro Bay. The maximum accretion value was 9.0 m and occurred near the mouth of the Pajaro River, just north of Moss Landing. This was an anomaly in an area of

mostly erosion: 98% of transects were erosional during the El Niño winter. In contrast, 49% of central California long-term (1998/2002-2016) transects were erosional. While central California saw the highest percentage of erosional transects during the El Niño winter, the data coverage during the winter of 2015/2016 is the lowest. Spatial distribution of NSM values and EPR values for central California can be seen in Figure 12(b).

Compared to northern and central California, southern California had the least extreme El Niño winter NSM mean of 9.7 m of erosion. The maximum winter erosion value was 112.7 m, which was the lowest maximum erosion value out of the three regions. This erosion value occurred at Monarch Beach, near Dana Point (Figure S1). The maximum accretion value was 62.3 m and occurred on the north side of the jetty at Newport Harbor in Newport Beach (Figure S2). For southern California 79% of NSM transects were found to be erosional during the El Niño winter. The long-term (EPR) 1998/2002-2016 percentages were less extreme in southern California, with 48% of transects eroding and 52% accretional or stationary transects. Spatial distribution of NSM values and EPR values for southern California can be seen in Figure 12(c and d).

### **Wave Energy Correlation**

The statewide relationship between cumulative wave energy flux ( $E_f$ ) and net shoreline movement during the El Niño winter is depicted in Figure 13. A Pearson correlation coefficient of  $r = -0.43$  ( $P < 0.001$ ) was found for the relationship between these two variables statewide, where  $N = 5520$  NSM (onshore) points, each with a corresponding  $E_f$  point (20 m depth). Thus,  $E_f$  and net shoreline movement during the El Niño winter of 2015/2016 are significantly (negatively) correlated across the state of California. The root-mean square error (RMSE) of the modeled line of best fit is equal to 18.5 m.

The relationship between normalized cumulative wave energy flux values ( $E_{f_{norm}}$ ) and Net Shoreline Movement (NSM) during the El Niño winter in southern California is shown

in Figure 14. A Pearson correlation coefficient of -0.23 ( $P < 0.001$ ) was found, indicating a significant correlation between  $E_{f_{norm}}$  and NSM, given  $N=4596$ . The root-mean square error (RMSE) of the modeled line of best fit is equal to 14.8 m. Many outliers beyond 14.8 m from the line of best fit were identified as shoreline change points in and around river mouths. Other outliers were identified as bordering human-made infrastructure such as jetties.

## **Discussion**

### **El Niño Change**

The magnitude and variability of shoreline response to the 2015/2016 El Niño across the state of California demonstrate the power of this record-breaking storm season and the vulnerability of California's beaches during strong El Niño events in the future. During the 2015/2016 El Niño winter, Central California experienced the highest percentage of eroding beaches and the most erosional mean shoreline change value of 98% and 45.5 m of erosion, respectively. Northern California had less erosion, with 89% of beaches eroding and a mean shoreline change value of 25.5 m of erosion. Southern California, while still experiencing severe erosion in many locations, had the lowest portion of eroding beaches (79%), and the least erosional mean of 9.7 m of erosion. The regional patterns observed here validate and expand upon the observations of Barnard et al. (2017), in which the most landward or eroded shoreline positions ever measured were observed in central and north-central California after the 2015/2016 winter. While central California's statistics were the most erosional out of the three regions, it is important to consider the limited data that were available in central California compared to the rest of the state (~52 km of beaches compared to ~76 km in northern California and ~280 km in southern California). While this could indicate that the observations in this study may not be representative of the entire central California region, it is notable that the presence of high-relief, cliff-backed coastline limits the quantity of sandy beaches available for analysis.

Figures 15(a) and 15(b) depict the rate and direction of change occurring across the state of California for EPR and NSM, respectively, along with the Universal Transverse Mercator (UTM) y-coordinate at which these changes are occurring. The NSM cumulative sum plot (Figure 15(a)) depicts one major change towards lower erosion rates at the division between central and southern California, and several other smaller slope fluctuations within each region. The degree of slope “flattening” between central and southern California reflects the more extreme erosion that occurred in northern and central California, compared to the southern region. It is noteworthy that a steepening of the southern California cumulative sum slope occurs south of the UTM y-coordinate of 3660000 northing, near Encinitas. This steepening indicates an increase in erosion as the coastline becomes primarily west-facing once again. Upon inspection of Figure 12(c), it is clear that south of this UTM y-coordinate, very little accretion occurred, but erosion up to 60 m occurred frequently.

Across the state, many erosional and accretional hotspots were seen at river mouths, such as Pudding Creek in Fort Bragg, Pismo River in Pismo Beach, and the Klamath River, where northern California’s highest accretional value was observed. While this could be due to increased precipitation during the El Niño storm season, as flooding can widen river outlets (Hart, 2009), precipitation levels during the 2015/2016 winter were not as anomalous as the winters of 1982/1983 and 1997/1998, particularly in southern and central California where drought persisted (Flick, 2016). More likely, these fluctuations are a result of wave refraction and the variation of alongshore sediment transport patterns near river outlets.

Within central and southern California, the highest erosional values were seen on the northern ends of westerly-facing beaches within embayments, such as in Monterey Bay, Morro Bay, and pocket beaches. The observations of this study are consistent with those of Young et al 2018, which concluded that during the 2015/2016 winter, pocket beaches in southern California saw erosion at the north (west) ends and accretion at the south (east) ends of beaches. Both studies observed this pattern around artificial structures as well, in which erosion was seen on the south (east) side and accretion on the north (west) side. This

pattern contrasts with the more typical El Niño pattern observed by Sallenger et al. (2002) during the extreme El Niño winter of 1997/1998, in which higher erosion was observed at the southern end of embayments, while accretion was observed at the northern end. This contrast in patterns can be attributed to the unique wave climate of the 2015/2016 El Niño winter, and emphasizes the impacts that an El Niño winter with primarily north-west swell can have on local erosional patterns (Figure 16). These patterns indicate the importance of wave orientation, in addition to wave energy, in shoreline erosion during an El Niño winter storm season and its influence on alongshore sediment transport across the coast of California.

Southern California's more southerly-facing orientation protects it from the more northerly wave direction that was documented in the region during the El Niño winter of 2015/2016, which contrasts to the southerly wave direction anomaly typical of previous El Niño winters (Barnard et al., 2017). The lower erosion values observed in southern California may be a result of this lack of southerly wave direction anomaly (and limited west-facing beaches in the northern part of the region), which served to shelter the coastline from wave energy. The combination of southern California's relatively low initial beach width and mild wave climate may have also influenced the less extreme erosion values observed in the region, as the beaches may lack the area and forcing conditions necessary to yield high erosion rates.

### **Long-term Change**

From 1998/2002 to 2016, southern and central California's shorelines were observed to be mostly stable, while northern California's shorelines were observed to be eroding at an average rate of 79 cm per year. It's notable that both mean EPR of shoreline change in central and southern California are slightly accretional, but the average change rates of both regions are very close to or within the EPR uncertainty bounds of those regions. Northern California is home to the highest percent of beaches that are eroding, and the lowest percent of beaches that are accreting out of the three regions. Figure 15(b) depicts long-term

fluctuations in erosion and accretion rates across the state. While there are many small-scale fluctuations between erosion and accretion in each of the three regions, the major changes in slope demonstrate a trend of erosion in northern California, stability in central California, and mild accretion in southern California. In southern California, many smaller-scale oscillations between erosional and accretional patterns are observed, occurring at ~25 to 50 km (500 to 1000 transect) intervals.

While The National Assessment of Shoreline Change (NASCH) rates (Hapke et al., 2006) have slightly different regional boundaries than those of this study, the longer timescales of their shoreline change analyses in California (1800s to 2002 linear regression rates of change and 1950s/1970s to 2002 end-point rates of change) motivate a comparison to the long-term rates of this study. Table 6 reveals details of both long-term and short-term NASCH rates of change. In northern California, long-term (1800s to 2002) NASCH rates are slightly accretional, short-term (1950s/1970s to 2002) NASCH rates are mostly stable, and the EPR (1998/2002-2016) presented here are slightly erosional. Our results could suggest a shift in northern California coastal geomorphology in recent years towards erosion. In central and southern California, both times periods of NASCH rates depict stable shorelines, which validate the stable shorelines observed from 1998/2002 to 2016 in this study.

The shift towards erosional shorelines in only northern California is surprising, considering the dramatic reduction in sediment supply that central and southern California have experienced due to coastal damming. From 1885-2008, the annual sand flux for the northern California rivers had only been reduced by about 5% as a result of coastal damming. In contrast, the central California sand flux had been reduced by 31%, and the southern California sand flux had been reduced by 50% (Slagel and Griggs, 2008). Rather than due to reduction in sediment supply, it is more likely that the shift towards erosion in northern California over the last two decades may be attributed to the more intense seasonal wave climate in northern California than the rest of the state. Evidence for this change is provided by the increase of multi-decadal wave height in the pacific northwest and the predicted

poleward migration of storm tracks on the North American west coast, which have indicated a northerly shift in the focus of extreme waves in 21st century projections (Barnard et al., 2017). The contrast in long-term rates between the north and south may also be attributed to the presence of coastal reinforcement structures in central and southern California and lack thereof in northern California. In particular, 38% of beaches in southern California were armored by 2018 (Griggs and Patsch, 2019), which effects a well-understood and documented process of passive erosion (Griggs, 2005).

Another significant driver to the long-term accretional patterns in the southern part of the state is the contribution of beach nourishment projects to local sediment budgets. Southern California received input of over 100 million cubic meters of sand to its littoral system from 1930 to 1993 (Flick, 1993), mainly in Santa Monica Bay. The combination of nourishment projects and retention structures can lead to sand permanence for decades (Pendleton et al., 2012), which is evident by visual inspection of long-term EPR and satellite imagery. However, it's important to note that because San Diego county has been the only location of major nourishment activity in the last few decades (Ludka et al., 2018), shore-normal retention structures (jetties, for example) are most likely the principle contributors to the long-term stability in the rest of the southern California region.

A comparison of the satellite-derived shoreline change rates (1984-2016) to the LiDAR-based EPR produced in this study reveals 22% more erosional transects statewide calculated via satellite-derived shorelines (Tables 4 and 5). The satellite-derived rates reveal similarly stable patterns in central and southern California and slightly different patterns in northern California. However, it should be noted that the same percentage of erosional transects is observed in northern California (70%) in both the satellite-derived rates and the EPR of this study. It's also important to consider that the satellite-derived mean change values of all three regions are slightly negative, but are within the uncertainty bounds of the rates ( $\pm 0.5\text{m}$ ) and therefore are considered stable shorelines. While these results do not agree with the erosional northern California EPR observed in this study, they are consistent

with this study's southern California EPR patterns. Additionally, the time period of the satellite change rates differs slightly from the time period of the EPR of this study, which may contribute to the differences seen.

It is important to consider that the seasonal variation of the shoreline is not included in any of the uncertainty values of the previously discussed shoreline change rates. For example, the NASCH rates of change assume that seasonal variability is negligible in the 1950s/1970s to 2002 end-point rates of change, and accounted for by the linear regression error of the 1800s to 2002 rates of change (Hapke et al., 2006). However, an end-point rate of change, such as the long-term rates in this study, may reflect the beach state during the time of data acquisition rather than a long-term trend. Thus, the long-term trends reported here should be considered speculative and provide incentive for further research, upon the availability of data with a higher temporal resolution.

### **EI Niño Wave Energy and Shoreline Change Correlation**

The cumulative wave energy flux ( $E_f$ ) anomaly during the El Niño winter of 2015/2016 is significantly correlated to increased erosion within the Southern California Bight. However, a stronger correlation was found between the 2015/2016 El Niño  $E_f$  (not normalized) and NSM across the state of California. Given the normalization of the cumulative wave energy flux values ( $E_{f_{norm}}$ ), removal of the NSM points that were directly influenced by river mouth output, and the higher model skill in Southern California Bight, one would expect to see a stronger correlation coefficient in the Southern California Bight analysis. Figure 14 demonstrates that regardless of the wave energy anomaly, most of the data in this analysis is clustered between 20 m of erosion and 20 m of accretion.

One possible explanation for the lower correlation between  $E_{f_{norm}}$  and NSM in the Southern California Bight is the influence of coastal orientation on wave sheltering and the protection from swell provided by offshore islands, particularly without the typical southerly wave direction that has been observed in previous El Niño winters. The wave climate within

the Southern California Bight is one of the most complicated in the world (Flick, 1993), which may result in discrepancies in wave hindcast results. Wave height and energy from the same offshore source can change considerably over a short distance before arriving at the beach (O'Reilly, 1993). Thus, there are likely instances in which wave hindcast estimates at the 20 m depth point are not representative of wave energy conditions at the corresponding mean high water point onshore.

Another potential explanation for the lower correlation seen in the Southern California Bight is the combination of initially low beach width and presence of human infrastructure in the region. For example, a seawall-backed beach will only erode as far back as the seawall will allow, regardless of wave energy, which explains the use of these structures for coastal protection. This concept is demonstrated in Figure S3. Visual inspection of shoreline change rates and satellite imagery show that low erosion rates are often seen in heavily armored areas. An example of this can be seen in Figure S4.

The investigation of outliers in the southern California  $Ef_{norm}$  and NSM plot (Figure 14) further reinforce the previously discussed idea of the influence of natural headlands and artificial coastal structures on erosional and accretional patterns in the region. Several extreme erosional outliers were identified as shoreline points located on the south side of impediments to littoral drift, while accretional outliers were identified to be on the north side of these structures. Examples of locations in which this pattern was observed include the groin field in Newport Beach (Figure S2) and the Camp Pendleton harbor near Oceanside.

## **Conclusions**

Extreme El Niño events have significant and potentially hazardous impacts on California's coastline, a coastline which is home to valuable infrastructure, communities, and ecosystems. A clearer understanding of the coastal dynamics that result from El Niño events is important for future planning and decision making in California's coastal zone. This study

was the first to investigate the impacts of the 2015/2016 El Niño, one of the strongest El Niño events of the last 145 years, on sandy beaches across the state of California.

Using LiDAR and ground-based GPS topographic data, over 400 km of sandy beaches along the length of the state's coast were analyzed to determine the shoreline change impacts of this powerful winter storm season. Central California experienced the most extreme sandy beach erosion during this time, followed by northern California and finally Southern California. Two main statewide shoreline change patterns were observed as a result of the El Niño winter: 1) high erosion and accretion near river mouths; and 2) accretion on the north side of structures impeding littoral drift (human-made or natural) paired with erosion on the south side of these structures. Additionally, in central California, higher erosion was observed at the northern ends of embayments (primarily on west-facing beaches) than on the southern ends. West-facing coastline in general experienced high erosion across the state.

From these observations, we infer that the net sand transport direction during this winter was from north to south, which is consistent with that of a typical (non-El Niño) winter. This transport direction may be explained by the lack of a statewide southerly wave direction anomaly during this El Niño winter in contrast to previous El Niño winters, where southerly anomalies were prevalent. These observations indicate the important role that wave direction played in the winter shoreline change observed and should be considered in future analyses of the impacts of El Niño on California's coastline. If this wave climate pattern persists, consistent with the observed poleward migration of storms tracks in recent decades, the dynamics of El Niño winter shoreline response may need to be reconsidered for future coastal management scenarios.

A significant correlation was found between cumulative wave energy flux and shoreline change during the El Niño winter across the state of California ( $R_2 = -0.45$ ,  $P < 0.001$ ). The correlation is lower ( $-0.25$ ,  $P < 0.001$ ) for the relationship between wave energy anomaly and shoreline change in southern California. The question remains as to whether or not the lower

correlation seen in southern California is due to lower average beach widths and the presence of human infrastructure inhibiting landward shoreline migration.

Over 600 km of sandy beaches across the state of California were analyzed to determine long-term (1998/2002-2016) shoreline change rates. In the long-term (1998/2002-2016) southern California and central California are mildly accreting, while northern California is eroding at an average rate of 79 cm per year. Northern California also has the highest proportion of beaches that are eroding, and the lowest proportion of beaches that are accreting compared to the rest of the state. The stability of southern California beaches may be attributed to a history of beach nourishment and shore-normal protection structures such as jetties and breakwaters in these regions. The lack of these human influences, combined with a more intense seasonal wave climate, may be the cause of more long-term shoreline change in northern California.

A useful future analysis would determine the percent of the initial beach width that was lost during the El Niño winter, and how these changes relate to mean wave direction and energy. Additionally, the need for collection of more spatially and temporally resolved LiDAR data encompassing shorelines during future El Niño winters remains. This, or the use of alternative data sources such as high-resolution satellite imagery, would allow for a more robust analysis of shoreline impacts across the state.

While long-term rates of sandy shoreline change will likely increase with sea-level rise, equally or more hazardous storm seasons (Ruggiero, 2013) will likely be more impactful in the coming decades, due to the extreme erosion caused during these storms. The potential doubling of occurrences of El Niño events due to greenhouse warming (Cai et al., 2014) alludes to the risks that California's shorelines will face in coming years due to El Niño winter storm events alone, which emphasizes the importance of understanding the impacts of these extreme events throughout coastal California.

**Supplemental Files List:**

Figure S1: 2015/2016 El Niño net shoreline movement interest area: Pudding Creek river mouth, Fort Bragg.

Figure S2: 2015/2016 El Niño net shoreline movement interest area: Monarch Beach.

Figure S3: 2015/2016 El Niño net shoreline movement interest area: Newport harbor.

Figure S4: 2015/2016 El Niño net shoreline movement interest area: Del Mar.

Figure S5: 2015/2016 El Niño net shoreline movement interest area: Playa del Ray.

## Bibliography

1. Allan, J.C., Komar, P.D., 2006. Climate Controls on US West Coast Erosion Processes. *J. Coast. Res.* 2006, 511–529.
2. Barnard, P.L., Allan, J., Hansen, J.E., Kaminsky, G.M., Ruggiero, P., Doria, A., 2011. The impact of the 2009-10 El Niño Modoki on U.S. West Coast beaches. *Geophys. Res. Lett.* 38, 1–7. <https://doi.org/10.1029/2011GL047707>
3. Barnard, P.L., Hoover, D., Hubbard, D.M., Snyder, A., Ludka, B.C., Allan, J., Kaminsky, G.M., Ruggiero, P., Gallien, T.W., Gabel, L., McCandless, D., Weiner, H.M., Cohn, N., Anderson, D.L., Serafin, K.A., 2017. Extreme oceanographic forcing and coastal response due to the 2015-2016 El Niño. *Nat. Commun.* 8. <https://doi.org/10.1038/ncomms14365>
4. Barnard, P.L., Short, A.D., Harley, M.D., Splinter, K.D., Vitousek, S., Turner, I.L., Allan, J., Banno, M., Bryan, K.R., Doria, A., Hansen, J.E., Kato, S., Kuriyama, Y., Randall-Goodwin, E., Ruggiero, P., Walker, I.J., Heathfield, D.K., 2015. Coastal vulnerability across the Pacific dominated by El Niño/Southern Oscillation. *Nat. Geosci.* 8, 801–807. <https://doi.org/10.1038/ngeo2539>
5. Barua, D.K., 2005. Wave Hindcasting. *Encycl. Coast. Sci. Encycl. Earth Sci. Ser.* [https://doi.org/10.1007/1-4020-3880-1\\_338](https://doi.org/10.1007/1-4020-3880-1_338)
6. Boak, E.H., Turner, I.L., 2005. Shoreline Definition and Detection: A Review. *J. Coast. Res.* 214, 688–703. <https://doi.org/10.2112/03-0071.1>
7. Cai, W., Borlace, S., Lengaigne, M., Van Rensch, P., Collins, M., Vecchi, G., Timmermann, A., Santoso, A., Mcphaden, M.J., Wu, L., England, M.H., Wang, G., Guilyardi, E., Jin, F.F., 2014. Increasing frequency of extreme El Niño events due to greenhouse warming. *Nat. Clim. Chang.* 4, 111–116. <https://doi.org/10.1038/nclimate2100>
8. Cayan, D., Kalansky, J., Pierce, D., 2018. California's Fourth Climate Change Assessment. La Jolla, California.
9. Colgan, C., Griggs, G., Hart, J.F., Hartge, E., Kudela, R., Mantua, N., Nielsen, K., 2018. California's Fourth Climate Change Assessment – Topical Reports TITLE California's Coast and Ocean Summary Report.
10. Dail, H.J., Merrifield, M.A., Bevis, M., 2000. Steep beach morphology changes due to energetic wave forcing. *Mar. Geol.* 162, 443–458. [https://doi.org/10.1016/S0025-3227\(99\)00072-9](https://doi.org/10.1016/S0025-3227(99)00072-9)
11. Esri Inc., 2017. ArcGIS Desktop 10.6.
12. Flick, R.E., 2016. California tides, sea level, and waves — Winter 2015-2016. *Shore & Beach* 84.
13. Flick, R.E., 1993. The Myth and Reality of Southern California Beaches. *Shore & Beach* 61, 15–16.

14. Google Earth Pro, 2016. State of California.
15. Griggs, G., 2005. the Impacts of Coastal Armoring. Shore and beach 13–22.
16. Griggs, G., Patsch, K., 2019. The Protection/Hardening of California’s Coast: Times Are Changing. *J. Coast. Res.* 35, 1051. <https://doi.org/10.2112/jcoastres-d-19a-00007.1>
17. Griggs, G., Patsch, K., Savoy, L., Flick, R., Fulton-Bennett, K., 2005. Living with the Changing California Coast, First. ed. University of California Press.
18. Hansen, J.E., Barnard, P.L., 2010. Sub-weekly to interannual variability of a high-energy shoreline. *Coast. Eng.* 57, 959–972. <https://doi.org/10.1016/j.coastaleng.2010.05.011>
19. Hapke, C.J., Reid, D., Richmond, B., 2009. Rates and Trends of Coastal Change in California and the Regional Behavior of the Beach and Cliff System. *J. Coast. Res.* 253, 603–615. <https://doi.org/10.2112/08-1006.1>
20. Hapke, C.J., Reid, D., Richmond, B.M., Ruggiero, P., List, J., 2006. National assessment of shoreline change, Part 3: Historical shoreline change and associated coastal land loss along sandy shorelines of the California coast, USGS Open File Report.
21. Hart, D.E., 2009. Morphodynamics of non-estuarine rivermouth lagoons on high-energy coasts. *J. Coast. Res.* 1355–1359.
22. Heberger, M., Cooley, H., Herrera, P., Gleick, P.H., Moore, E., 2011. Potential impacts of increased coastal flooding in California due to sea-level rise. *Clim. Change* 109, 229–249. <https://doi.org/10.1007/s10584-011-0308-1>
23. Himmelstoss, E.A., Henderson, R.E., Kratzmann, M.G., Farris, A.S., 2018. Digital Shoreline Analysis System (DSAS) version 5.0 user guide. Open-File Rep. <https://doi.org/10.3133/ofr20181179>
24. Huang, B., L’Heureux, M., Hu, Z.Z., Zhang, H.M., 2016. Ranking the strongest ENSO events while incorporating SST uncertainty. *Geophys. Res. Lett.* 43, 9165–9172. <https://doi.org/10.1002/2016GL070888>
25. Inman, D.L., Shepard, F.P., 1951. Nearshore Circulation, in: First Conference on Coastal Engineering. Scripps Institution of Oceanography, La Jolla, California, p. Chapter 5.
26. IPCC, 2007. Climate Change 2007: Impacts, Adaptation and Vulnerability., Contribution of Working Group II to the Fourth Assessment Report of the Intergovernmental Panel on Climate Change. Cambridge, UK. <https://doi.org/10.1029/93JC02439>
27. Ludka, B.C., Gallien, T.W., Crosby, S.C., Guza, R.T., 2016. Mid-El Niño erosion at nourished and unnourished Southern California beaches. *Geophys. Res. Lett.* 43, 4510–4516. <https://doi.org/10.1002/2016GL068612>

28. Ludka, B.C., Guza, R.T., O'Reilly, W.C., 2018. Nourishment evolution and impacts at four southern California beaches: A sand volume analysis. *Coast. Eng.* 136, 96–105. <https://doi.org/10.1016/j.coastaleng.2018.02.003>
29. Luijendijk, A., Hagenaars, G., Ranasinghe, R., Baart, F., Donchyts, G., Aarninkhof, S., 2018. The State of the World's Beaches. *Sci. Rep.* 8, 6641. <https://doi.org/10.1038/s41598-018-24630-6>
30. Moore, L.J., Ruggiero, P., List, J.H., 2006. Comparing Mean High Water and High Water Line Shorelines: Should Proxy-Datum Offsets be Incorporated into Shoreline Change Analysis? *J. Coast. Res.* 224, 894–905. <https://doi.org/10.2112/04-0401.1>
31. Myers, M.R., Barnard, P.L., Beighley, E., Cayan, D.R., Dugan, J.E., Feng, D., Hubbard, D.M., Iacobellis, S.F., Melack, J.M., Page, H.M., 2019. A multidisciplinary coastal vulnerability assessment for local government focused on ecosystems, Santa Barbara area, California. *Ocean Coast. Manag.* 104921. <https://doi.org/10.1016/j.ocecoaman.2019.104921>
32. National Oceanic and Atmospheric Administration (NOAA), 2019. NOAA Tides and Currents: Tidal Datums [WWW Document]. URL <https://oceanservice.noaa.gov/privacy.html> (accessed 10.7.19).
33. NOAA National Weather Service Climate Prediction Center, 2019. Cold & Warm Episodes by Season [WWW Document]. URL [https://origin.cpc.ncep.noaa.gov/products/analysis\\_monitoring/ensostuff/ONI\\_v5.php](https://origin.cpc.ncep.noaa.gov/products/analysis_monitoring/ensostuff/ONI_v5.php)
34. NOAA Office for Coastal Management, 2019. NOAA Digital Coast [WWW Document]. URL <https://coast.noaa.gov/digitalcoast/data/home.html>
35. O'Reilly, W., 1993. The Southern California Wave Climate: Effects of Islands and Bathymetry. *Shore & Beach* 61.
36. O'Reilly, W.C., Olfe, C.B., Thomas, J., Seymour, R.J., Guza, R.T., 2016. The California coastal wave monitoring and prediction system. *Coast. Eng.* 116, 118–132. <https://doi.org/10.1016/j.coastaleng.2016.06.005>
37. Pendleton, L., Mohn, C., Vaughn, R.K., King, P., Zoulas, J.G., 2012. Size matters: The economic value of beach Erosion and Nourishment in Southern California. *Contemp. Econ. Policy* 30, 223–237. <https://doi.org/10.1111/j.1465-7287.2011.00257.x>
38. Philander, S.G.H., 1983. Anomalous El Nino of 1982-83. *Nature* 305, 16. <https://doi.org/10.1038/305016a0>
39. Previsic, M., 2006. CALIFORNIA OCEAN WAVE ENERGY ASSESSMENT. <https://doi.org/CEC-500-2006-119>
40. Ruggiero, P., 2013. Is the Intensifying Wave Climate of the U . S . Paci fi c Northwest Increasing Flooding and Erosion Risk Faster Than Sea-Level Rise ? 139, 88–97. [https://doi.org/10.1061/\(ASCE\)WW.1943-5460.0000172](https://doi.org/10.1061/(ASCE)WW.1943-5460.0000172)
41. Sallenger, A.H., Krabill, W., Brock, J., Swift, R., Manizade, S., Stockdon, H., 2002.

- Sea-cliff erosion as a function of beach changes and extreme wave runup during the 1997-1998 El Niño. *Mar. Geol.* 187, 279–297. [https://doi.org/10.1016/S0025-3227\(02\)00316-X](https://doi.org/10.1016/S0025-3227(02)00316-X)
42. Santoso, A., Mcphaden, M.J., Cai, W., 2017. The Defining Characteristics of ENSO Extremes and the Strong 2015/2016 El Niño. *Rev. Geophys.* <https://doi.org/10.1002/2017RG000560>
  43. Seymour, R.J., 1998. Effects of El Niños on the West Coast Wave Climate. *Shore & Beach* 66, 3–6.
  44. Slagel, M.J., Griggs, G.B., 2008. Cumulative Losses of Sand to the California Coast by Dam Impoundment. *J. Coast. Res.* 243, 571–584. <https://doi.org/10.2112/06-0640.1>
  45. Storlazzi, C., Wingfield, D., 2005. Spatial and Temporal Variations in Oceanographic and Meteorologic Forcing Along the Central California Coast , 1980 – 2002, Scientific Investigations Report.
  46. Storlazzi, C.D., Griggs, G.B., 2000. Influence of El Niño-Southern Oscillation (ENSO) events on the evolution of Central California's shoreline. *Bull. Geol. Soc. Am.* 112, 236–249. [https://doi.org/10.1130/0016-7606\(2000\)112<236:IOENOE>2.0.CO;2](https://doi.org/10.1130/0016-7606(2000)112<236:IOENOE>2.0.CO;2)
  47. Taylor, J.R., 1982. An introduction to error analysis: The study of uncertainties in physical measurements. University Science Books, Mill Valley, California.
  48. U.S. Bureau of Economic Analysis, 2019. Gross Domestic Product: First quarter 2019. <https://doi.org/10.4135/9781412952422.n129>
  49. Vos, R., Velasco, M., De Labastida, E., 1999. Economic and Social Effects of El Niño in Ecuador Sustainable Development Department Technical Papers Series.
  50. Weber, K.M., List, J.H., Morgan, K.L.M., 2005. U.S. Geological Survey Open-File Report 2005-1027: An Operational Mean High Water Datum for Determination of Shoreline Position from Topographic Lidar Data.
  51. Wilson, G.W., Fischetti, T.R., 2010. Coastline Population Trends in the United States : 1960 to 2008. U. S. Census Bur. 1–28.
  52. Wolter, K., Timlin, M.S., 2011. El Niño Southern Oscillation behaviour since 1871 as diagnosed in an extended multivariate ENSO index (MEI.ext). *Int. J. Climatol.* 1087, 1074–1087. <https://doi.org/10.1002/joc.2336>
  53. Young, A.P., Flick, R.E., Gallien, T.W., Giddings, S.N., Guza, R.T., Harvey, M., Lenain, L., Ludka, B.C., Melville, W.K., O'Reilly, W.C., 2018a. Southern California Coastal Response to the 2015–2016 El Niño. *J. Geophys. Res. Earth Surf.* 123, 3069–3083. <https://doi.org/10.1029/2018JF004771>
  54. Young, A.P., Flick, R.E., Gallien, T.W., Giddings, S.N., Guza, R.T., Harvey, M., Lenain, L., Ludka, B.C., Melville, W.K., O'Reilly, W.C., 2018b. Data from: Southern California Coastal Response to the 2015-16 El Niño [WWW Document]. UC San Diego Libr. Digit. Collect.

## Figures

Figure 1: Oceanographic forcing anomalies along the US West Coast. Top: Winter (December through February) anomaly (change) in mean wave energy flux relative to the winter mean from 1997–2019. The anomaly of the top 5% (that is, ‘elevated’) of the winter wave energy flux relative to the mean of all winters is plotted with squares. Bottom: Wave direction anomalies. Anomaly in winter mean peak wave direction (+ is North, - is South) relative to the overall winter mean. The wave direction anomaly for the top 5% of the winter wave-energy flux measurements from the top panel are plotted with squares (wave data sources: <http://cdip.ucsd.edu>; <http://www.ndbc.noaa.gov/>). Note the legend placed in the top figure also refers to the buoy locations in the bottom. Figure modified from Barnard et al. 2017.

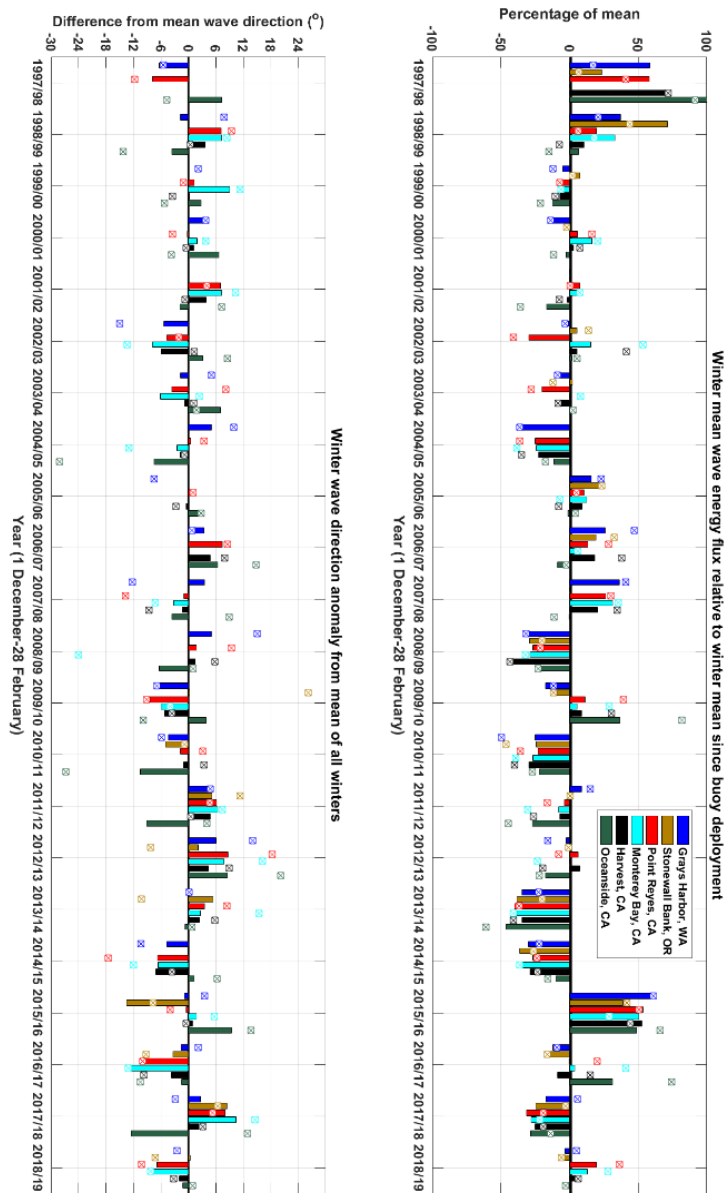


Figure 2: Locations of buoys used to predict and validate nearshore wave parameters along the California coast. The California coastal wave monitoring and prediction system estimates wave conditions at the 20-m depth contour, based on deep-water directional offshore buoys. The non-stationary, linear, spatial refraction model estimates spectral parameters, which are validated against nearshore buoy observations when available. All buoys are Datawell Directional Waveriders, except 46022 and 4602 (NOAA 3 m discus buoys)(O'Reilly et al., 2016).

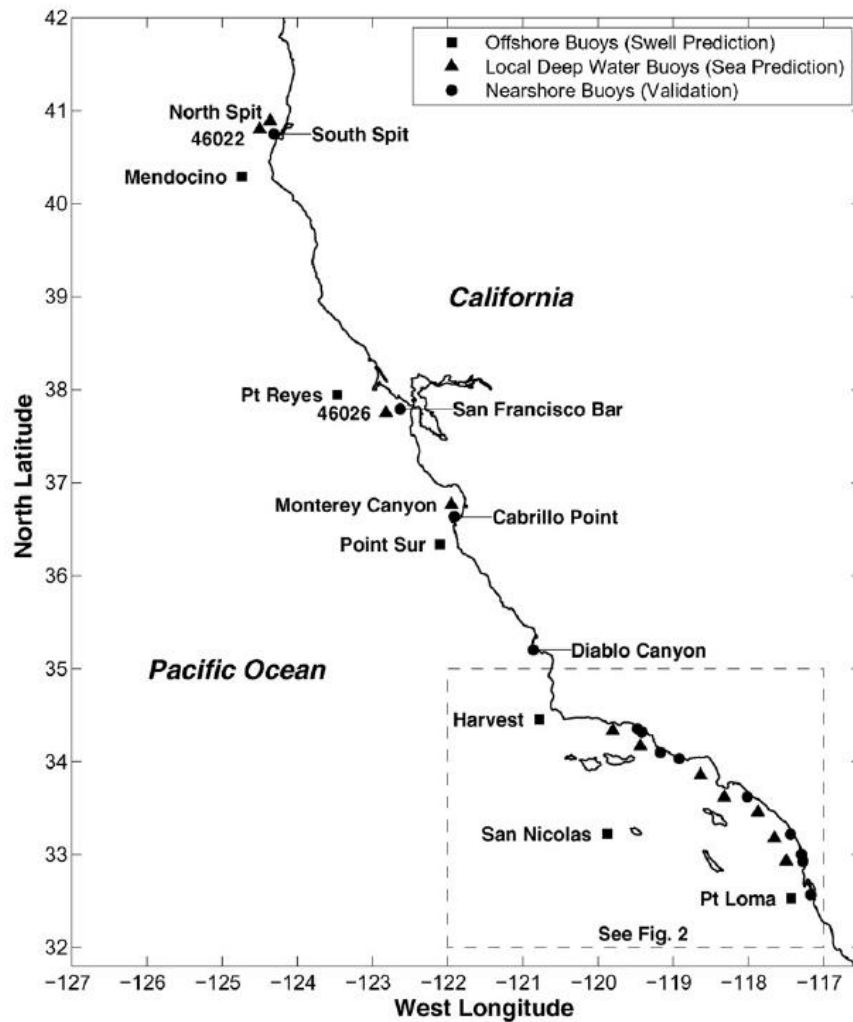


Table 1: Data sources and associated uncertainty values for the long and short-term shoreline change analysis. Regional names are abbreviated.

Data Sources and Shoreline Uncertainty Values ( $\sigma$ s)								
						Total Shoreline Positional Uncertainty ( $\sigma$ s)(m)		
Data Source	Year	Coverage	DEM Vertical Uncertainty (m)	DEM Horizontal Uncertainty (m)	$\sigma$ s NorCal	$\sigma$ s CenCal	$\sigma$ s SoCal	
1	1998 Spring West Coast: Post-El Nino Lidar DEM	1998	CenCal, SoCal	0.15	0.8	N/A	2.28	1.84
2	2002 NASA/USGS Pacific Coast Shoreline Lidar DEM	2002	NorCal	0.15	0.8	2.1	N/A	N/A
3	2015 USACE NCMP Topobathy Lidar DEM	2015	Statewide	0.196	1	4.06	4.35	4.13
4	USGS PCMSC Topographic GPS Surveys	2015	Northern Monterey Bay, Ocean Beach	N/A	N/A	N/A	0.28	N/A
5	UCSD DEM: Southern California Coastal Response to the 2015-16 El Niño	2015	SoCal	0.024	0.112	N/A	N/A	0.45
6	2016 USGS West Coast El-Nino Lidar DEM	2016	Statewide	0.06	0.21	0.74	0.72	0.7

Figure 3: Spatial coverage of the different data sources used across the state of California and their associated net shoreline movement (NSM) uncertainty values in meters. Refer to Table 1 for details on each source number.



Figure 1: Regional boundaries determined by this study and mean high water (MHW) elevation boundaries determined by the National Assessment of shoreline change (Hapke et al. 2006).

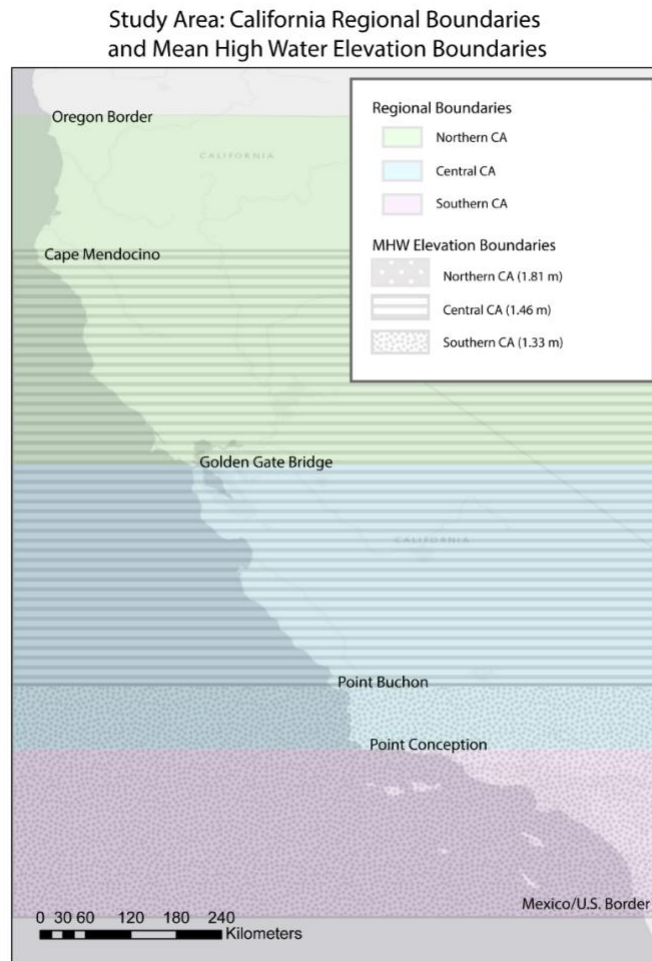


Table 2: Mean high water (MHW) elevations for each region and associated tidal gauge measurements. Original table from Hapke et al. (2006), original values from (Moore, Ruggiero, & List, 2006).

	Site Name	MHW above NAVD88 (m)	Average of MHW
Northern California	Crescent City, CA	1.80 m	1.81
	Trinidad Bay, CA	1.76 m	
	Port Orford, OR	1.87 m	
Central California	Arena Cove, CA	1.52	1.46
	Point Reyes, CA	1.49	
	Monterey Harbor, CA	1.40	
	San Simeon, CA	1.43	
Southern California	Port San Luis, CA	1.37	1.33
	Santa Barbara, CA	1.35	
	Rincon Island, CA	1.34	
	Santa Monica, CA	1.35	
	Huntington Beach, CA	1.32	
	La Jolla, CA	1.28	
Imperial Beach, CA	1.33		

Figure 5: Spatial variation of uncertainty values associated with long-term (1998-2016) end-point rates of shoreline change.

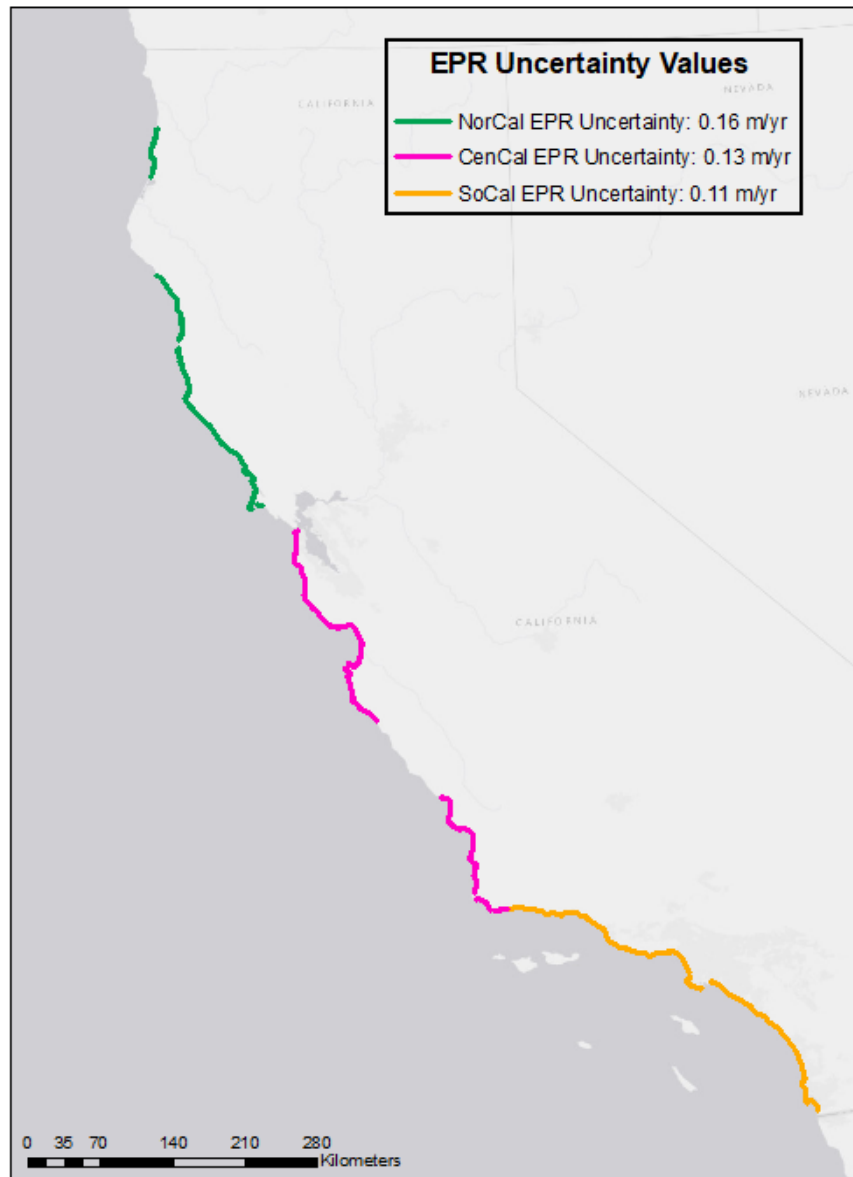


Figure 6: Statewide locations of 2015/2016 El Niño net shoreline movement transects. Negative values indicate erosion.

2015/2016 El Niño Winter Net Shoreline Movement Statewide Transects

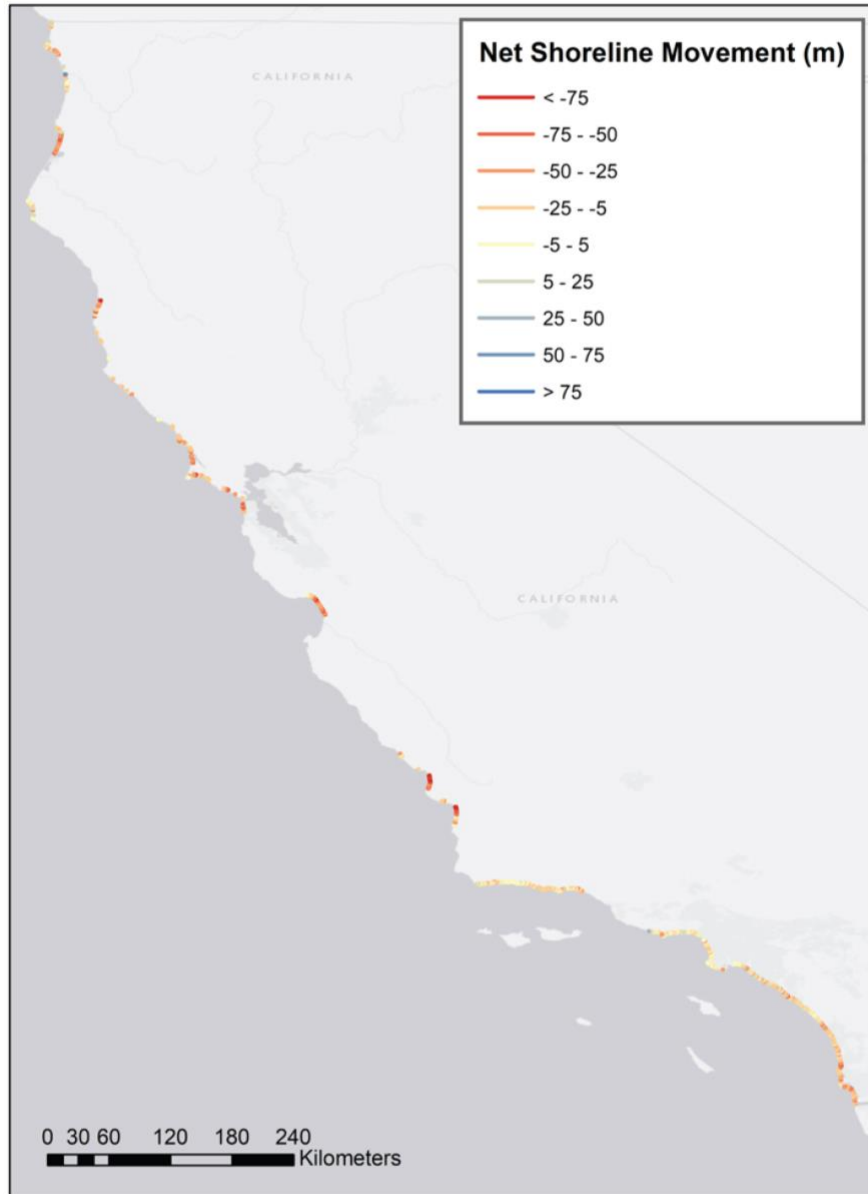


Figure 7: Northern California locations of 2015/2016 El Niño net shoreline movement transects. Negative values indicate erosion.

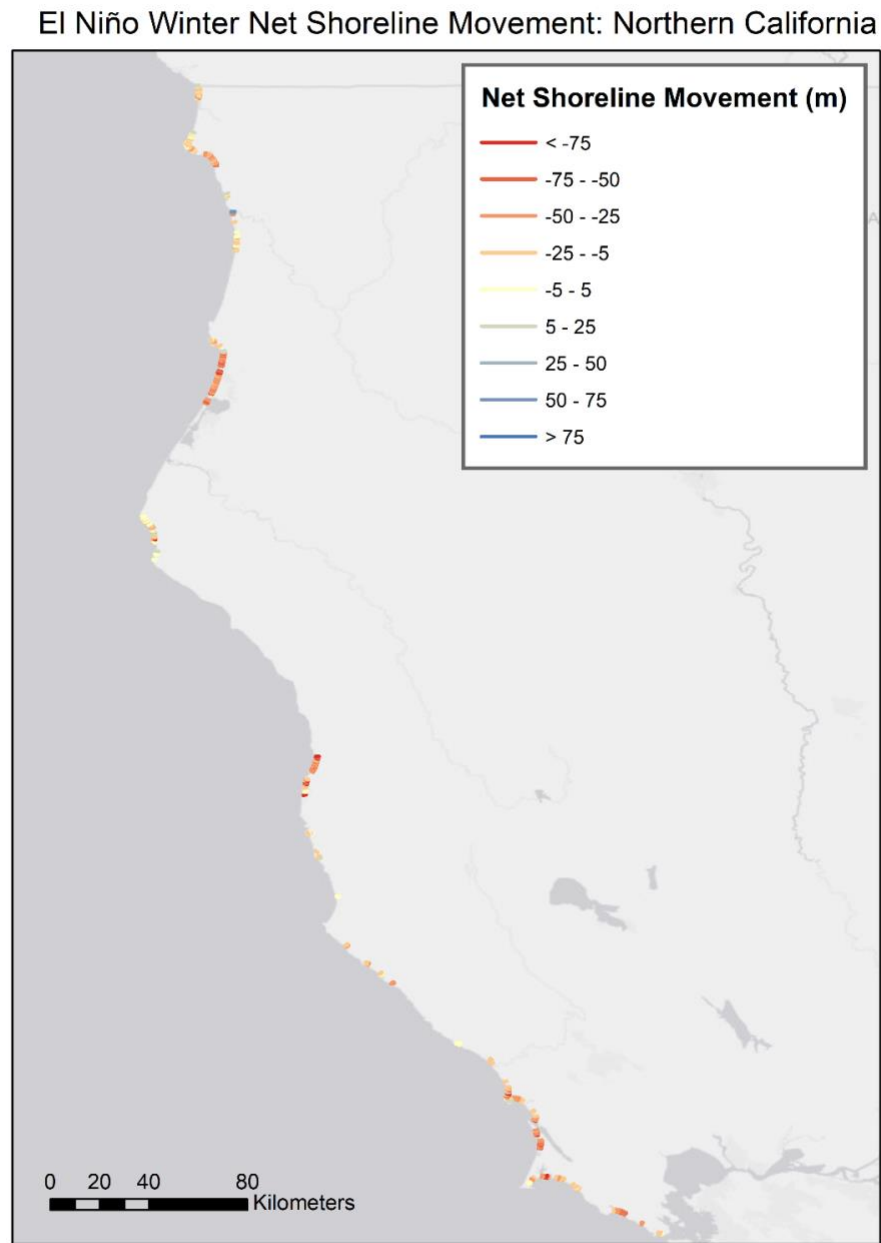


Figure 8: Central California locations of 2015/2016 El Niño net shoreline movement transects. Negative values indicate erosion.

### El Niño Winter Net Shoreline Movement: Central California

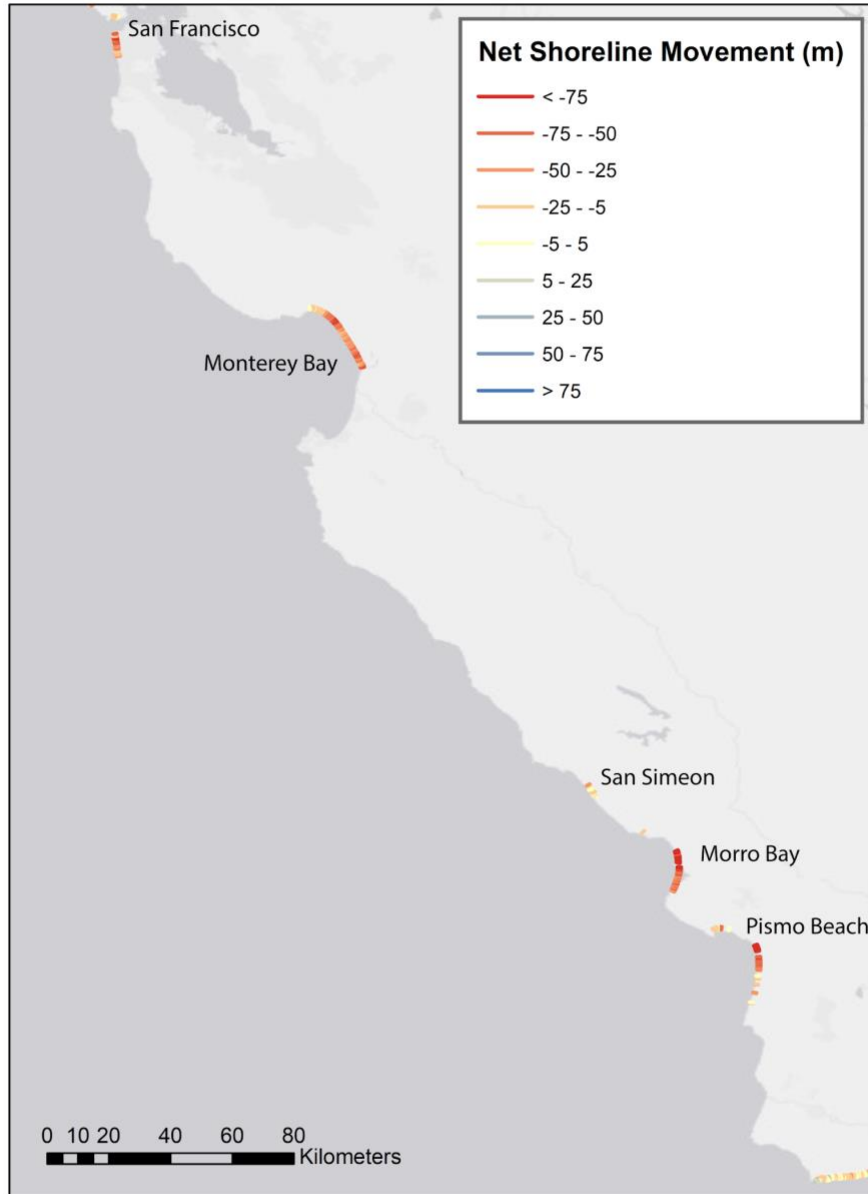


Figure 9: Southern California locations of 2015/2016 El Niño net shoreline movement transects. Negative values indicate erosion.

### El Niño Winter Net Shoreline Movement: Southern California

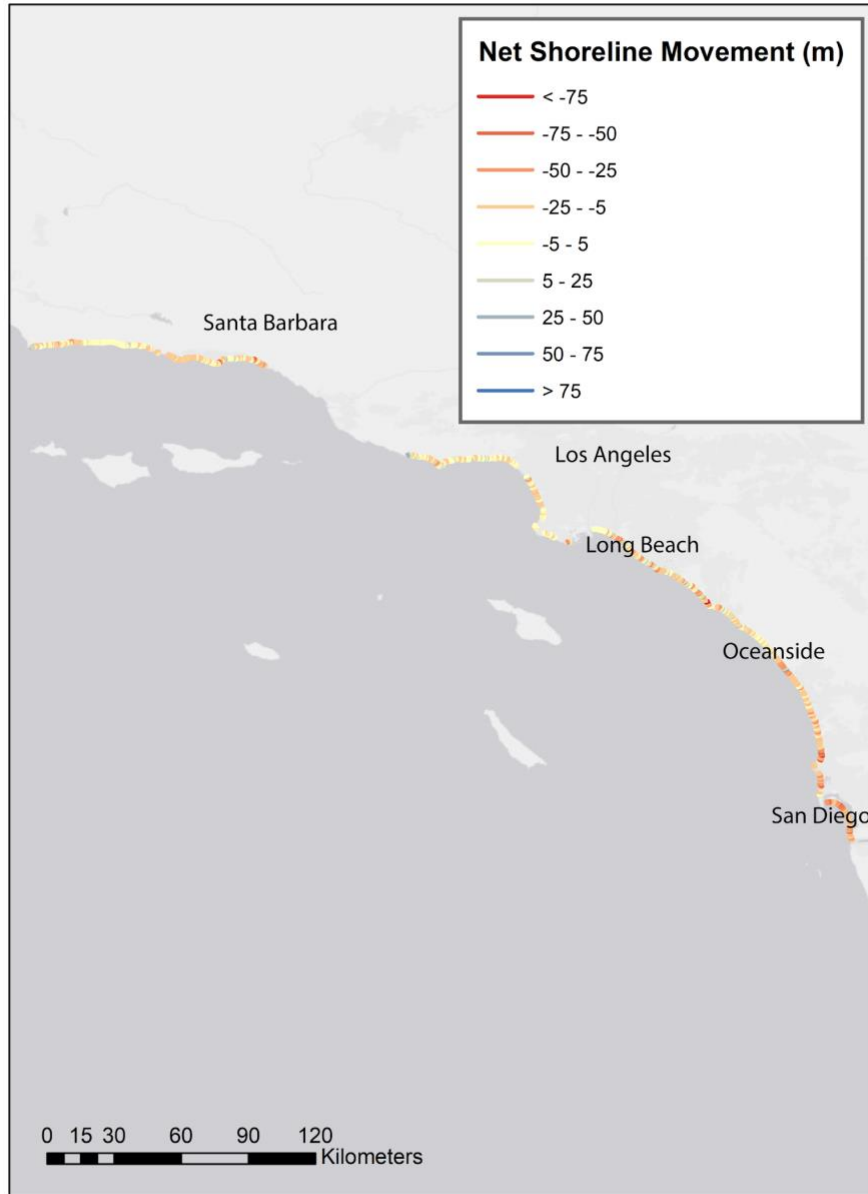


Table 3: Summary of statistics related to net shoreline motion values for the El Niño winter. The 2015 data source column refers to the numbering in Table 1: Data Sources and Shoreline Uncertainty Values.

2015/2016 El Niño Winter Net Shoreline Motion (NSM) Statistics												
Region	Transect Count	Analysis Coverage (km)	Erosional Average	Erosional Maximum	Accretional Average	Accretional Maximum	Mean	Standard Deviation	% Erosional Transects	% Accretional Transects	NSM Uncertainty (m)	2015 Data Source Reference
NorCal	1524	76.2	-30	-148.6	10.8	61.9	-25.5	23.1	89	11	4.13	#3
CenCal	1033	51.65	-46.46	-121.02	2.28	8.95	-45.7	26	98	2	0.77 4.41	#4 #3
SoCal	5616	280.8	-14.21	-112.7	7.12	62.3	-9.7	15.7	79	21	0.83 4.19	#5 #3
Statewide	8173	408.65	-22.16		7.5		-17.2	22.6	83	17	N/A	N/A

Table 4: Summary of statistics related to end-point rates of shoreline change from 1998-2016

1998-2016 End Point Rate (EPR) Statistics									
Region	Transect Count	Analysis Coverage (km)	Mean	Standard Deviation	% Erosional Transects	Accretional or Stationary Transects	Accretional or Stationary Mean	Erosional Mean	EPR Annualized Uncertainty (m/yr)
NorCal	2025	101.25	-0.79	1.87	70	30	1.27	-1.67	0.16
CenCal	3722	186.1	0.08	1.07	49	51	0.89	-0.72	0.13
SoCal	6821	341.05	0.15	0.98	48	52	0.75	-0.52	0.11
Statewide	12568	628.4	-0.02	1.24	52	48	0.85	-0.82	N/A

Table 5: Summary of statistics related to the satellite-derived long-term rates of shoreline change. Statewide rates of change provided by Luijendijk et al. (2018).

1984-2016 Satellite Derived Linear Regression Rate of Shoreline Change Statistics								
Region	Transect Count	Analysis Coverage (km)	Mean (m/yr)	% Erosional Transects	% Accretional or Stationary Transects	Accretional or Stationary Mean (m/yr)	Erosional Mean (m/yr)	Uncertainty (m/yr)
NorCal	1570	785	-0.2	69.6	30.4	1.51	-0.95	0.5
CenCal	1214	607	-0.46	81.3	18.7	0.83	-0.77	
SoCal	1030	515	-0.32	73.2	26.8	0.84	-0.74	
Statewide	3814	1907	-0.32	74.3	25.7	1.17	-0.83	

Table 6: Summary of National Assessment rates of shoreline change. Long-term (1800s-2002) is abbreviated as LT. Short-term (1950s/1970s - 2002) is abbreviated as ST. Shoreline change rates produced by Hapke et al. (2006).

Short-term and Long-term National Assessment Shoreline Change Statistics												
Region	Transect Count		Mean (m/yr)		% Erosion		% Accretion		Accretional Mean (m/yr)		Erosional Mean (m/yr)	
	LT	ST	LT	ST	LT	ST	LT	ST	LT	ST	LT	ST
NorCal	2966	3364	0.5 +/- 0.1	0.3 +/- 0.4	23	47	77	53	0.7 +/- 0.1	1.2 +/- 0.4	-0.3 +/- 0.1	-0.6 +/- 0.4
CenCal	5982	6478	0.0 +/- 0.1	-0.5 +/- 0.4	53	79	47	21	0.2 +/- 0.1	0.6 +/- 0.4	-0.3 +/- 0.1	-0.8 +/- 0.4
SoCal	5614	6300	0.3 +/- 0.1	-0.1 +/- 0.4	36	64	64	35	0.6 +/- 0.1	0.9 +/- 0.4	-0.2 +/- 0.1	-0.8 +/- 0.4

Figure 10: Distribution of 2015/2016 El Niño winter net shoreline movement values within **a)** northern California **b)** central California, and **c)** southern California. The mean change value is plotted on each subplot, along with the average of all negative change values in each region (erosional average) and the average of all positive change values in each region (accretional average). For regional boundary descriptions, see figure 4.

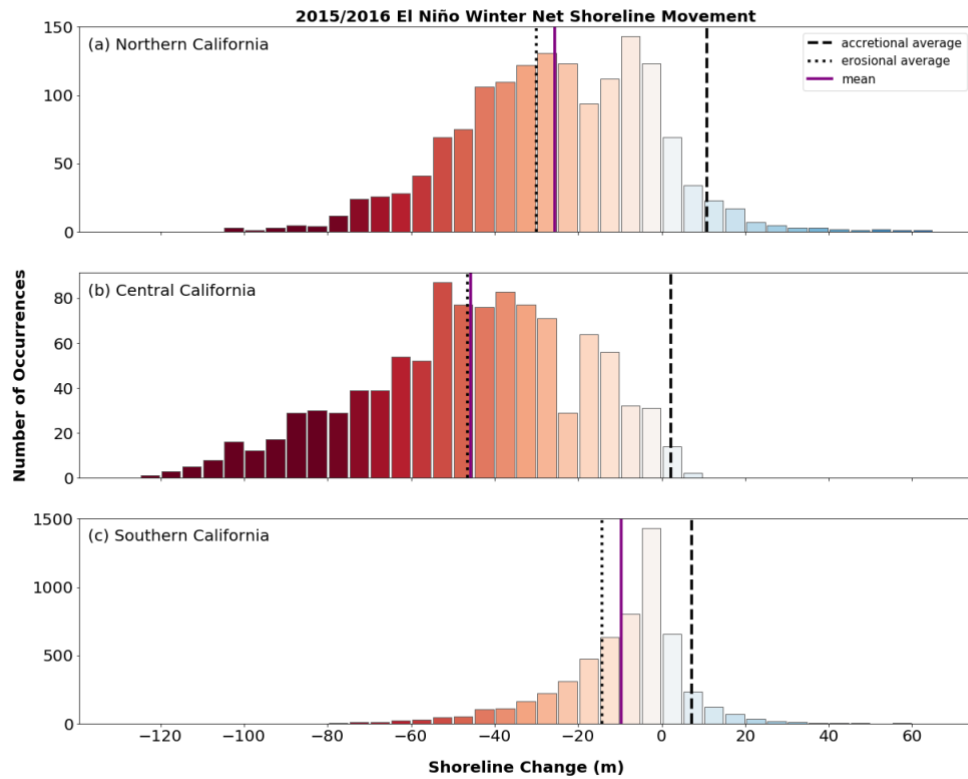


Figure 11: Distribution of 1998-2016 end-point rates of shoreline change within **a)** northern California **b)** central California, and **c)** southern California. The mean change value is plotted on each subplot, along with the average of all negative change values in each region (erosional average) and the average of all positive change values in each region (accretional average). For regional boundary descriptions, see figure 4.

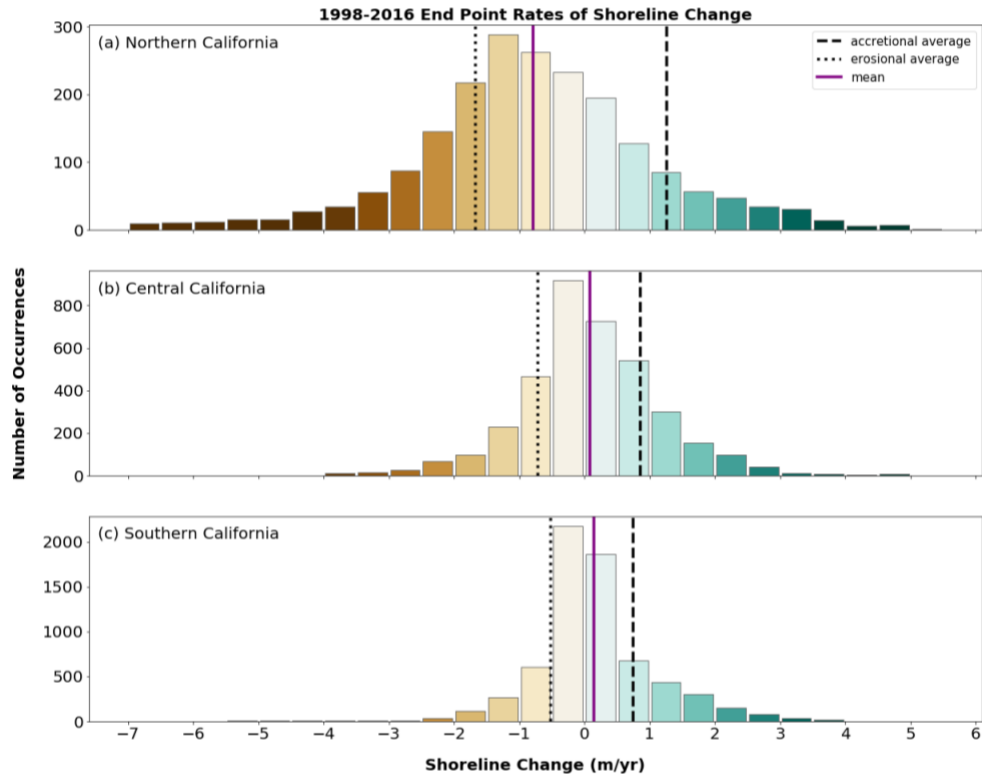
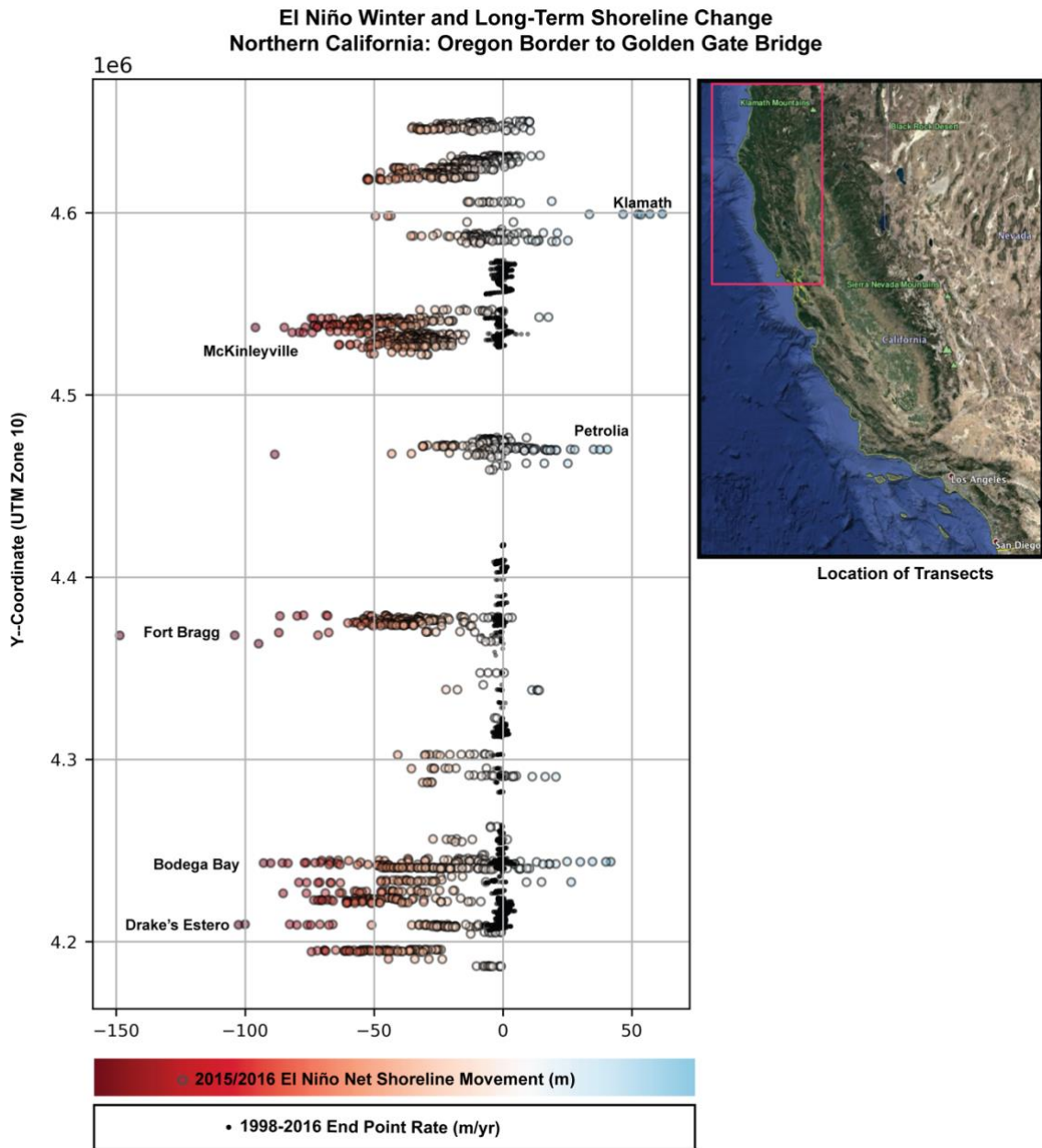
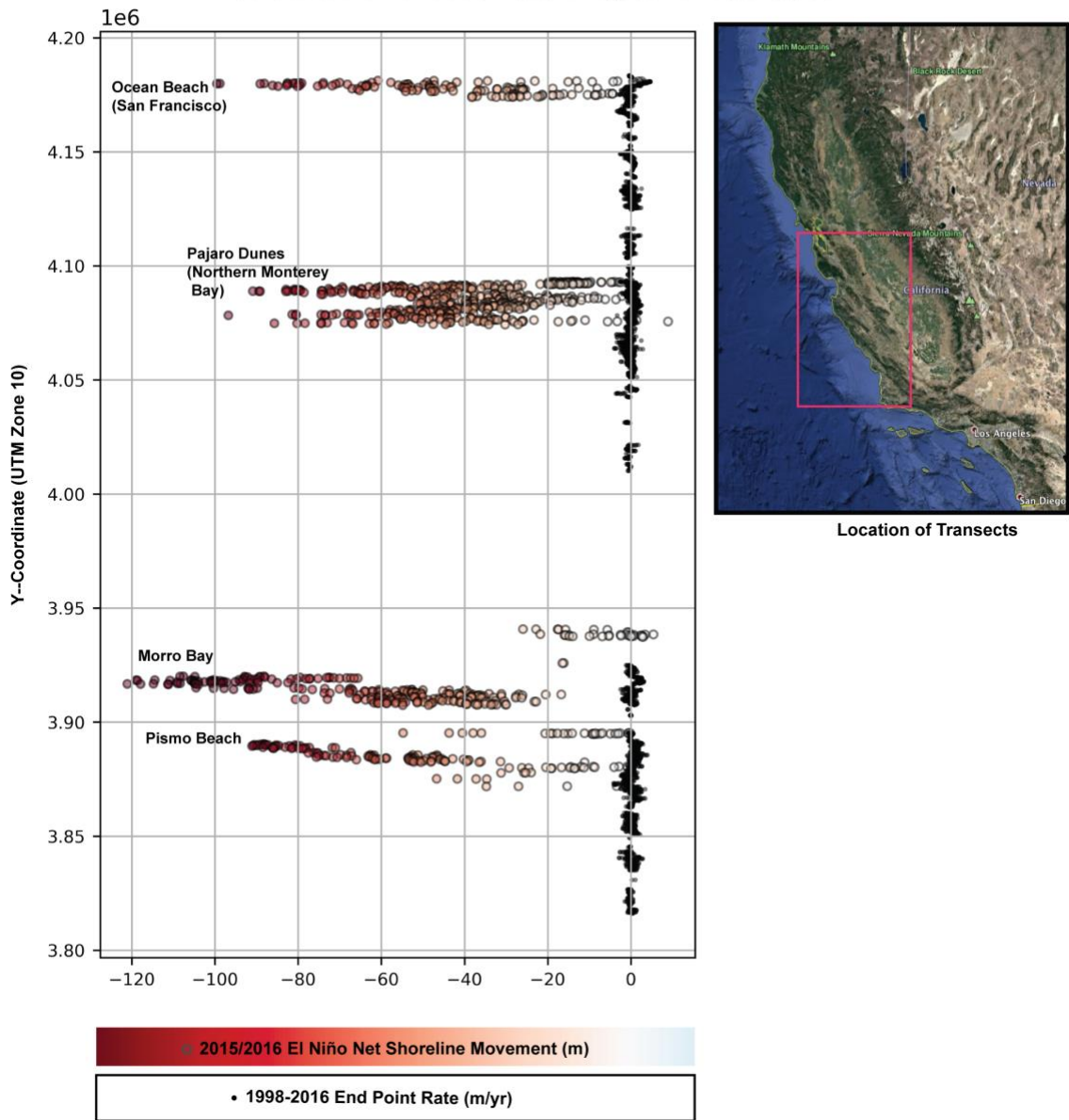


Figure 12: Distribution of 2015/2016 El Niño winter net shoreline movement (NSM) change values and long-term end-point rates of shoreline change in relation to northing (UTM Y-coordinate) for: **a)** Northern California, **b)** Central California, **c)** Southern California's south-facing coastline, **d)** Southern California's west facing coastline. Labels of locations are approximate and intended to depict general locations of extreme El Niño change and provide reference to general areas of change. For uncertainty values, see tables 3 and 4. Reference map: California imagery from Google Earth Pro 7.3.2.5491, 2018, accessed 11/01/2019. <https://www.google.com/earth/versions/>.



**El Niño Winter and Long-Term Shoreline Change  
Central California: Golden Gate Bridge to Point Conception**



**Figure 12(b)**

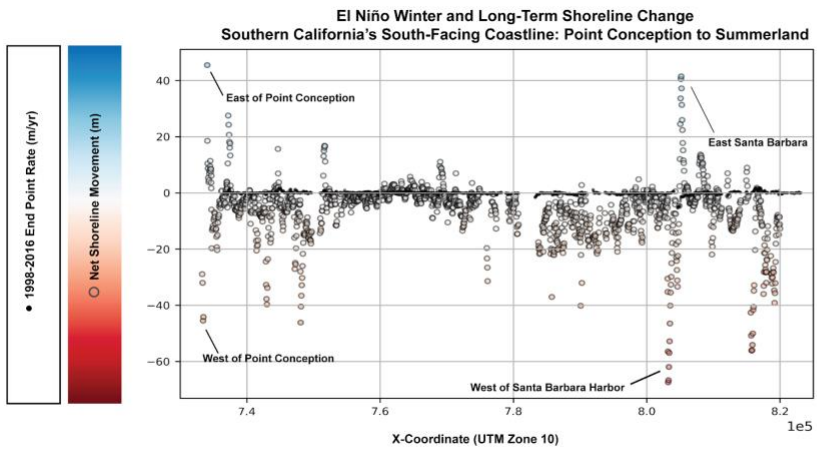


**Figure 12(c)**

**El Niño Winter and Long-Term Shoreline Change  
Southern California: Summerland to U.S./Mexico Border**

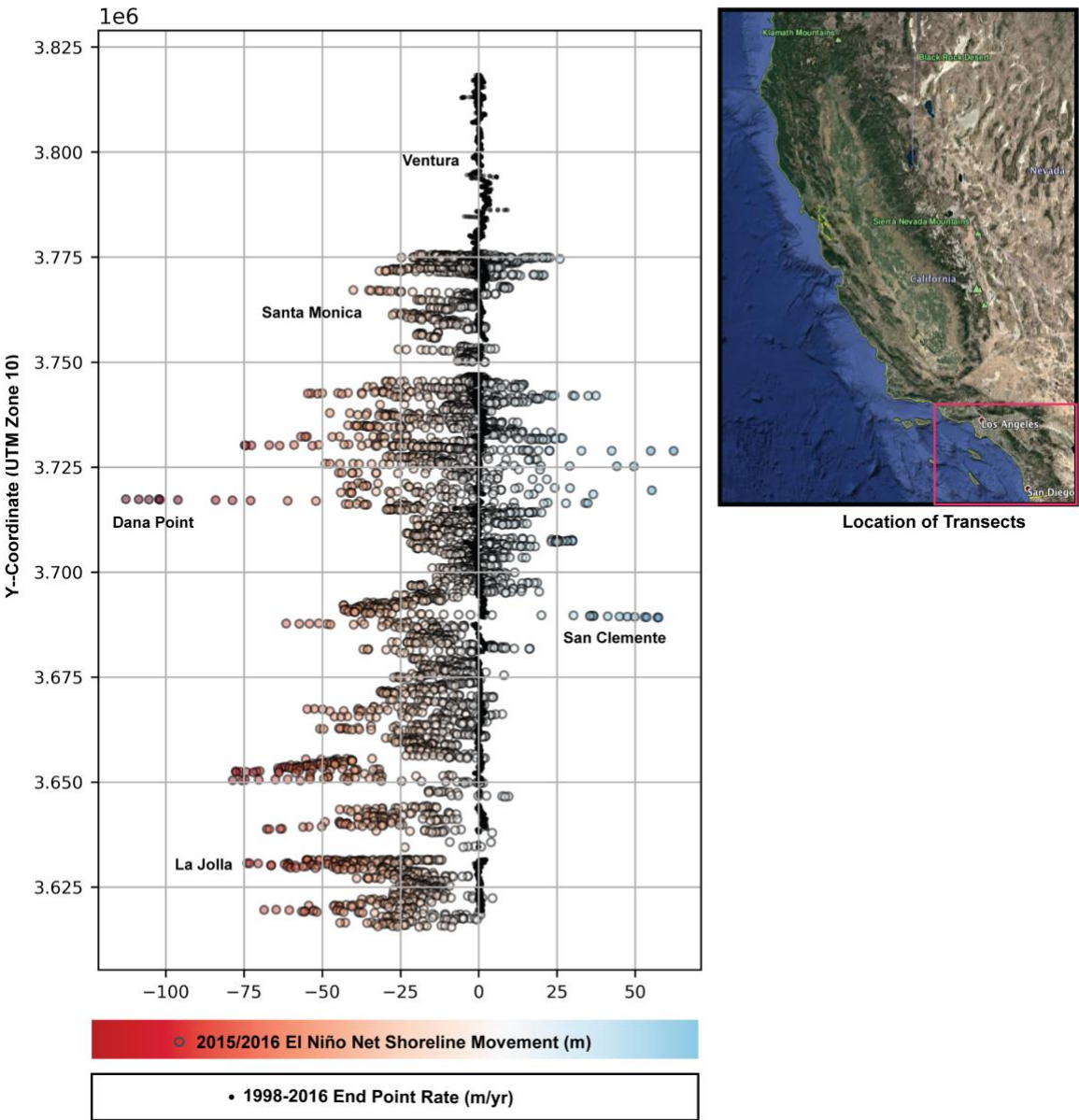


**Figure 12(d)**

Figure 13: A statistically significant relationship exists between cumulative wave energy flux and net shoreline movement during the 2015/2016 El Niño winter across the state of California, given  $R=-0.45$  and  $P<0.001$ . Cumulative wave energy flux values were calculated hourly from August 2015 to April 2016 at 100 m transects at the 20 m depth using hindcast data from the California coastal wave monitoring and prediction system (O'Reilly et al., 2016). For more details on the analysis, see methods.

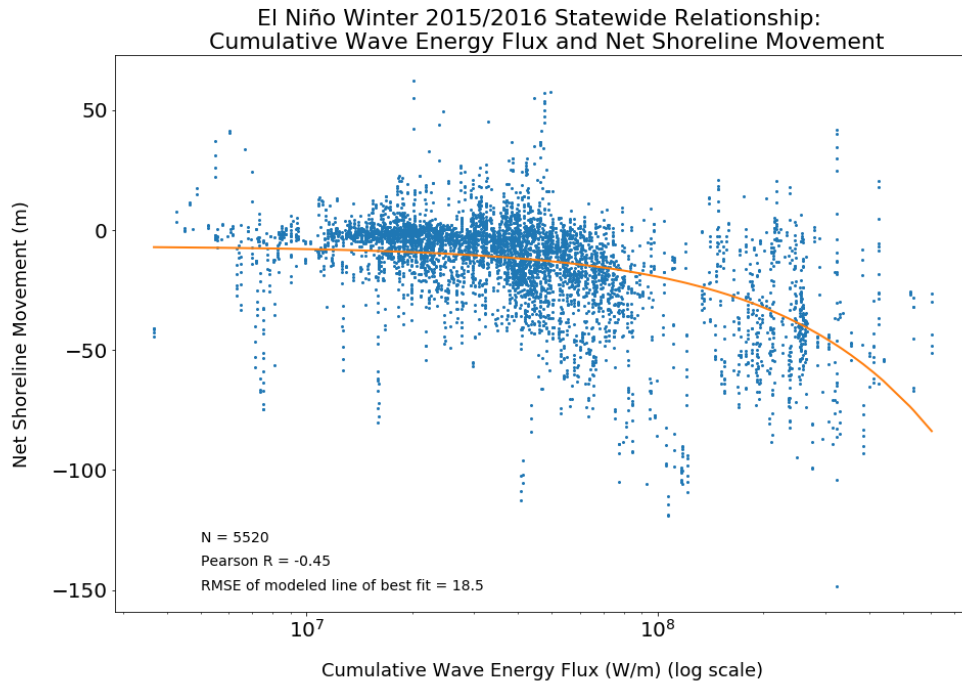


Figure 14: **Left:** Within the southern California bight, A statistically significant relationship exists between the 2015/2016 winter cumulative wave energy flux anomaly and net shoreline movement during the 2015/2016 El Niño winter, given  $R=-0.25$  and  $P<0.001$ . Cumulative wave energy flux values were calculated hourly from August 2015 to April 2016 at 100m transects, at the 20 m depth, using hindcast data from the California coastal wave monitoring and prediction system (O'Reilly et al., 2016). Outliers representing 1.5% of the filtered dataset were eliminated by filtering for pairs of points in which the wave energy anomaly was less than 0.7, and for shoreline points located at river mouths. For more details on the analysis, see methods. **Right:** Locations of NSM points used for this analysis.

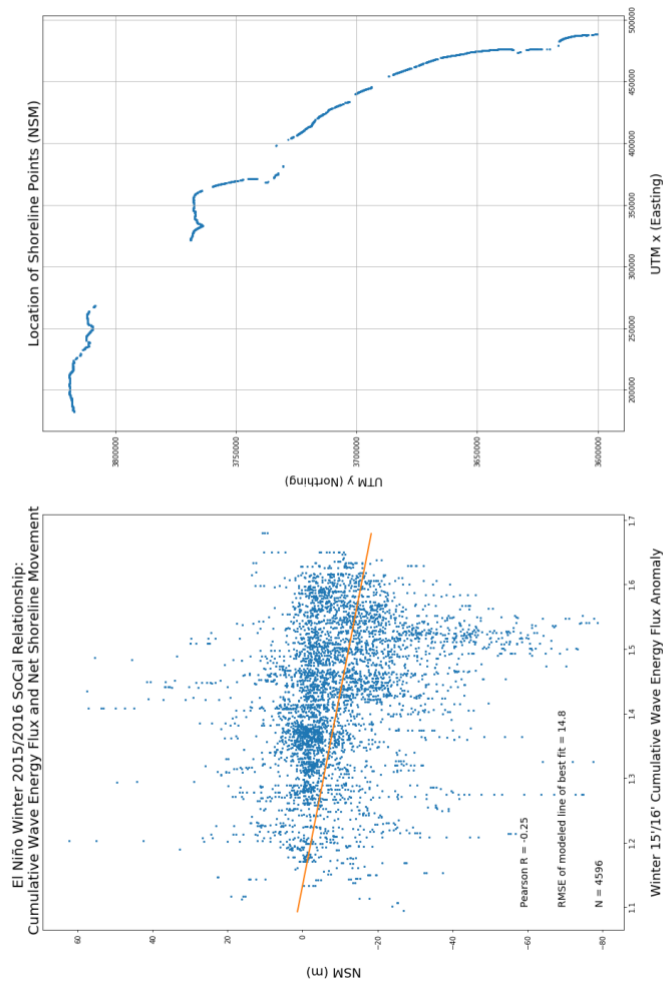


Figure 15: Cumulative sum plots of a) net shoreline movement during the El Niño winter of 2015/016 and b) end-point rates of shoreline change between 1998 and 2016. The rate and direction (accretional or erosional) of shoreline change across the state of California is shown by the blue line, while the UTM y-coordinate at which the blue line occurs is shown in orange. Transect ID (different for EPR and NSM) is displayed on the x-axis and is plotted from north at TID 1 to south at TID 8000 (NSM) or 12000 (EPR). Shore-normal transects are spaced at 50 m alongshore and located based on presence of a sandy beach and availability of data and are therefore not continuous alongshore. Gaps in data are visible as vertical segments of the UTM y-coordinate line (in orange). Changes in the slope of the blue line are interpreted as changes in erosional or accretional trends in an area and are labeled in a). For more details on slope breaks, see discussion section.

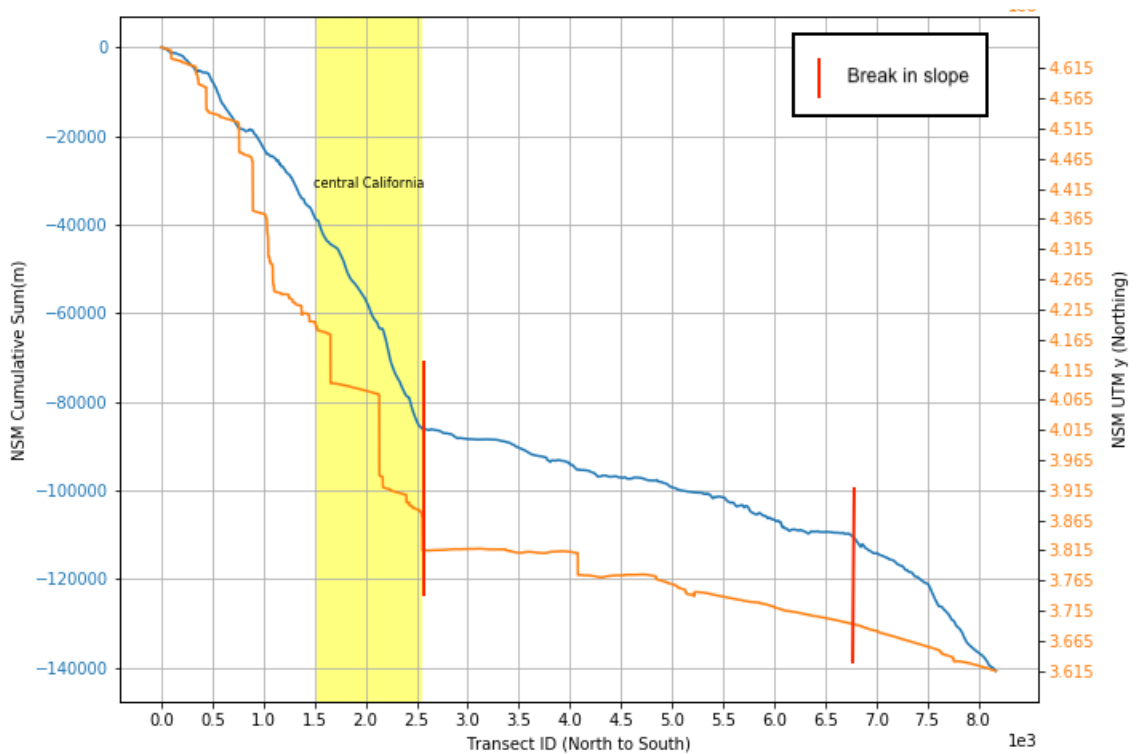


Figure 15(a)

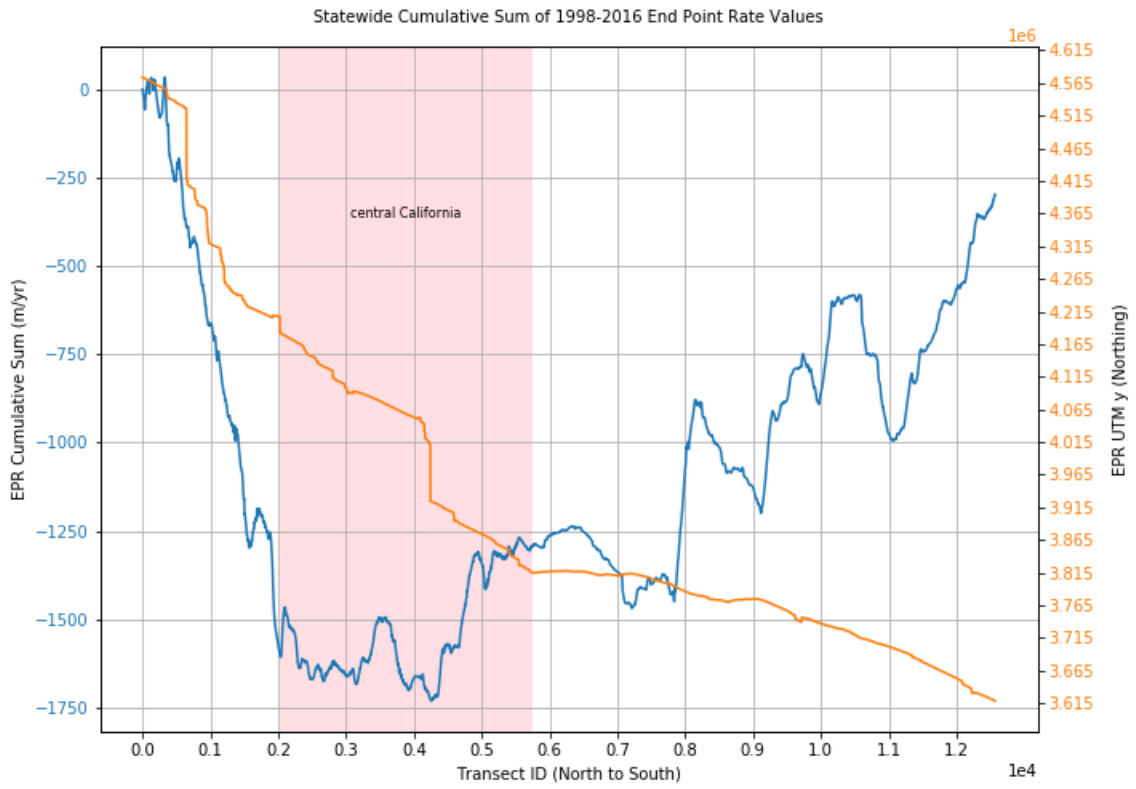


Figure 15(b)

Figure 16: 2015/2016 El Niño winter net shoreline movement values (onshore) and cumulative wave energy flux values (offshore) during the approximate winter shoreline change period (August 2015 through April 2016). The presence of low wave energy near high erosion rates may indicate the importance of wave direction, rather than power, in the erosional patterns observed within embayments. The northwesterly wave direction observed during the 2015/2016 El Niño helps to explain the pattern of high erosion in the northern end of embayments, and low erosion in the southern end.

### 2015/2016 El Niño Winter Net Shoreline Movement and Cumulative Wave Energy Flux



**Supplementary Materials:**

**2015/2016 El Niño Winter Net Shoreline Movement:  
Erosion at Mouth of Salt Creek: Monarch Beach**



Figure S1: Net shoreline movement interest area: The maximum southern California erosion value during the El Niño winter of 2015/2016 in occurred at Monarch Beach near Dana Point, reaching -112.7 m of erosion.

2015/2016 El Niño Winter Net Shoreline Movement:  
Maximum Statewide Accretion: Newport Harbor



Figure S2: Net shoreline movement interest area: The maximum statewide accretion value during the El Niño winter of 2015/2016 occurred near Newport Harbor in central California, where accretion on the north side of the harbor reached 62.3 m.

## 2015/2016 El Niño Winter Net Shoreline Movement: Erosion to Back Beach Barrier: Del Mar

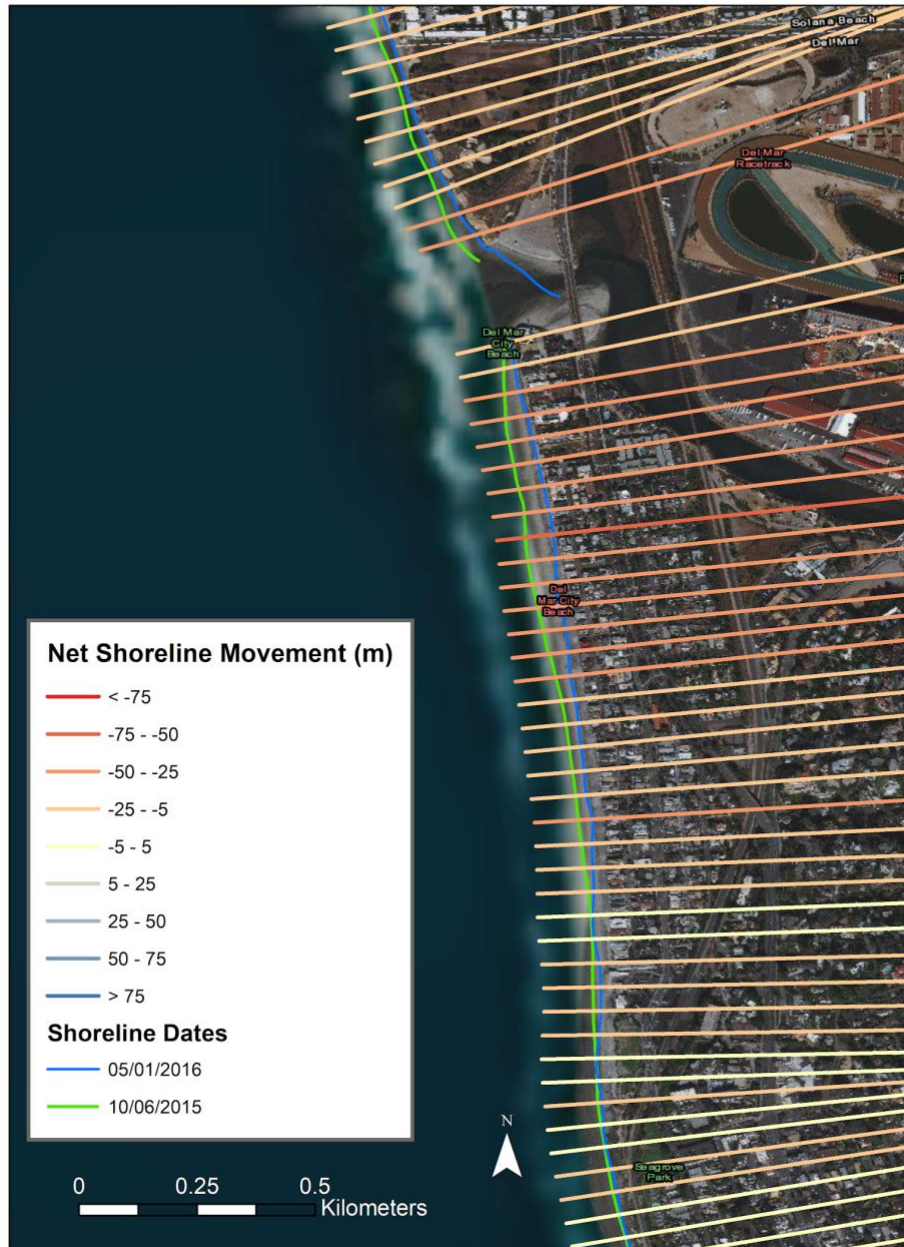


Figure S3: Net shoreline movement interest area: During the El Niño winter of 2015/2016, the maximum possible beach erosion occurred, reaching the edge of the back-beach barrier in Del Mar, southern California. In this case, the back-beach barrier is human-made infrastructure.

## 2015/2016 El Niño Winter Net Shoreline Movement: Armored Playa Del Rey Beaches

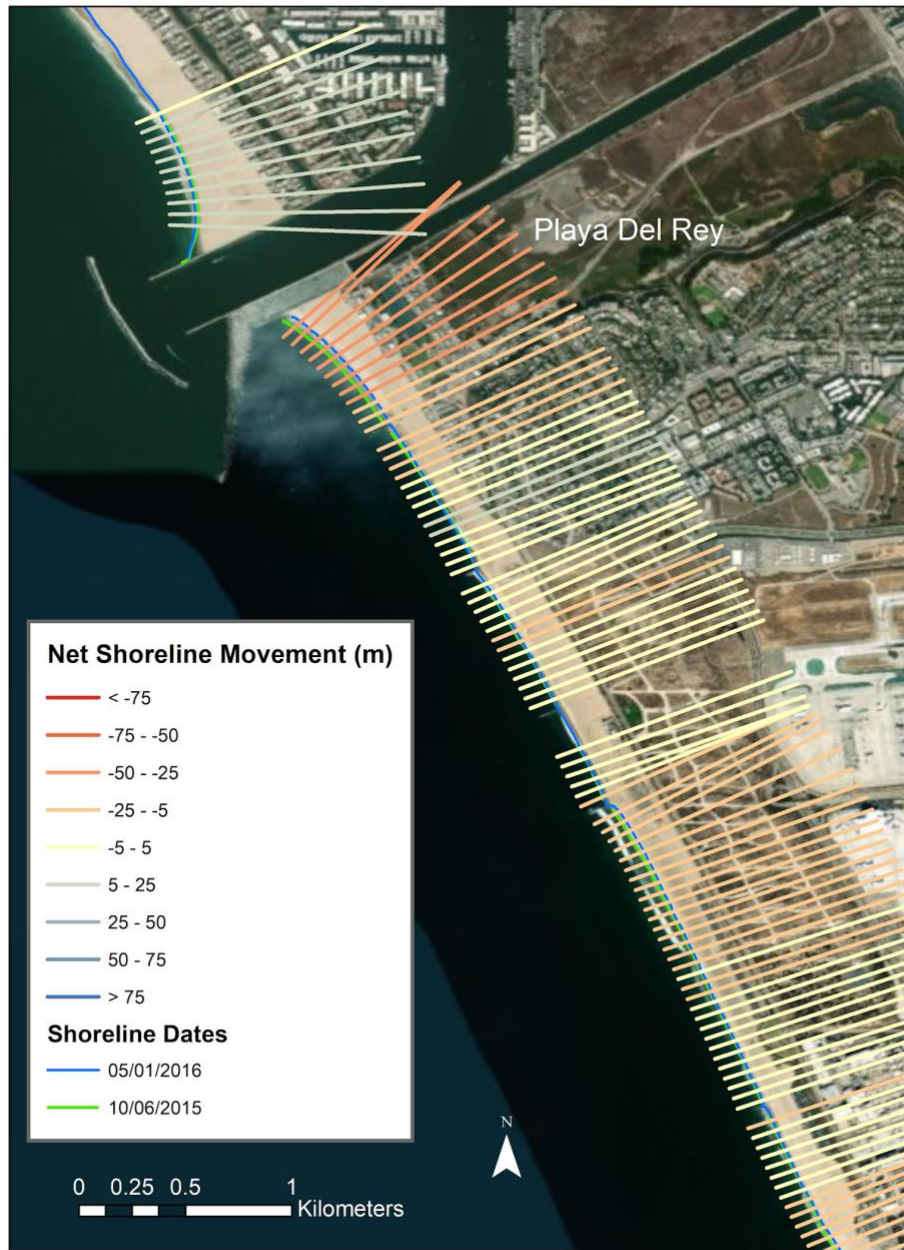


Figure S4: Net shoreline movement interest area: Playa Del Rey, in southern California, experienced relatively less erosion during the El Niño winter of 2015/2016 than other beaches in the state. Visual inspection of shoreline change rates and satellite imagery shows that often low erosion rates are seen in heavily structured areas.